energy&fuels

Article

pubs.acs.org/EF

Confined Pyrolysis for Simulating Hydrocarbon Generation from Jurassic Coaly Source Rocks in the Junggar Basin, Northwest China

Hao Xu,[†] Xianghua Ding,[‡] Zhengjiang Luo,[‡] Cuimin Liu,[‡] Erting Li,[‡] Pan Huang,[†] Shuang Yu,[†] Jinzhong Liu,[†] Yanrong Zou,[†] and Changchun Pan*[,†]

[†]State Key Laboratory of Organic Geochemistry, Guangzhou Institute of Geochemistry, Chinese Academy of Sciences, Wushan, Guangzhou 510640, China

[‡]Research Institute of Experiment and Testing, Xinjiang Oilfield Company, PetroChina, Karamay, Xinjiang 834000, China

Supporting Information

ABSTRACT: Several oil and gas fields have been found in which oil and gas were mainly derived from the Jurassic coaly source rocks in the Junggar Basin, northwest China. Pyrolysis experiments were performed on two coals (J23C1 and FM1C2) and one type III kerogen of mudstone (Di9S1) from Jurassic strata in the basin at two heating rates of 20 and 2 °C/h in confined systems (gold capsules). Hydrogen indices and H/C atomic ratios of the three samples J23C1, FM1C2, and Di9S1 are 83, 197, and 226 mg/g TOC, and 0.70, 0.86, and 1.01, respectively. The measured maximum oil yields for the three samples are 59.37, 175.75, and 80.75 mg/g TOC, respectively, inconsistent with hydrogen indices and H/C atomic ratios. However, the measured maximum gas yields ($\sum C_{1-5}$) for the three samples are 90.69, 157.24, and 198.15 mg/g TOC, respectively, consistent with hydrogen indices and H/C atomic ratios. This result is interpreted by kerogen Di9S1 containing mainly crossed alkane moieties with both terminals attached to aromatic rings while coals J23C1 and FM1C2 contain mainly alkane moieties with only one terminal attached to an aromatic ring based on kerogen ^{13}C NMR spectra and the oil yield relative to gas yield and compositions of liquid components produced in confined pyrolysis. The crossed alkane moieties were hardly released as liquid alkanes but likely further cracked into gaseous components during pyrolysis. Jurassic strata contain some effective oil source rocks which produced enough amount of oil required for oil expulsion and formation of commercial oil reservoirs in oil generative window (Ro 0.6−1.35%). The amounts of gaseous hydrocarbons generated from the Jurassic coaly source rocks are generally low in oil generative window due to low transformation ratios. Elevated maturity (Ro > 1.35%) is a critical controlling factor to the Jurassic coaly source rocks generating sufficient gaseous hydrocarbons and forming commercial gas reservoirs.

1. INTRODUCTION

Oil and gas generation from coals has been heavily studied since the 1980s, or even earlier.[1,2] Hunt[3] suggested the coals which have higher H/C atomic ratio (>0.9) and Rock-Eval hydrogen indices (HI > 200 mg HC/g TOC) are capable of generating oil. These coals are generally characterized with high amounts of liptinite and alginite macerals at low maturity.[2−17] Peters[18] suggested that the generative potential of liquid hydrocarbons from coals is commonly overestimated by Rock-Eval pyrolysis and is best determined by elemental analysis and organic petrography. The latter studies by Isaksen et al.[19] and Killops et al.[20] demonstrated that bulk parameters, such as H/C atomic ratio and HI value, are not effective indicators of the oil generative potential of coals and terrigenous organic matter, and there appears to be no association between maceral content and amount of nonvolatile oil expelled from coals. Sykes and Snowdon[21] suggested that the maturation characteristics of coaly source rocks are fundamentally different from those of marine and lacustrine rocks, and warrant separate guidelines for Rock-Eval-based assessment of their petroleum generative potential and thermal maturity. Dieckmann et al.[22] and Erdmann and Horsfield[23] documented that the recombination reactions of liquid products released from type III kerogen at low levels of maturation result in the formation of a thermally stable bitumen, which is the major source of methane at very high maturity, and emphasized that these recombination reactions can be only simulated in closed system pyrolysis.

Several oil and gas fields have been found in which oil and gas were mainly derived from the Jurassic coaly source rocks in the Junggar Basin, northwest China.[24−30] Previous studies demonstrated that coal measures are the most important source rocks for hydrocarbon gases in Chinese gas fields, especially the giant ones with gas reserve > 100 billion cubic meters.[31,32] These giant gas fields with hydrocarbon gases derived from coals and coaly rocks mainly occur in three regions, i.e., Ordos Basin, Kuqa Depression of Tarim Basin, and Sichuan Basin.[32] However, the results of exploration activities for gas reservoirs differ substantially among coal-bearing basins in China. Song et al.[33] estimated that the reserves of gaseous hydrocarbons found so far occupy about 14.1% and 2.2%, respectively, of those predicted in the Kuqa depression of the Tarim Basin and southern Junggar Basin, which were derived from coal measures. Exploration for coal gas reservoirs has been very successful in the Kuqa depression of Tarim Basin.[34] However, it is somewhat disappointing in the central and southern Junggar Basin.[35]

Received: May 12, 2016
Revised: October 9, 2016
Published: December 1, 2016

ACS Publications © 2016 American Chemical Society

DOI: 10.1021/acs.energyfuels.6b01143
Energy Fuels 2017, 31, 73−94

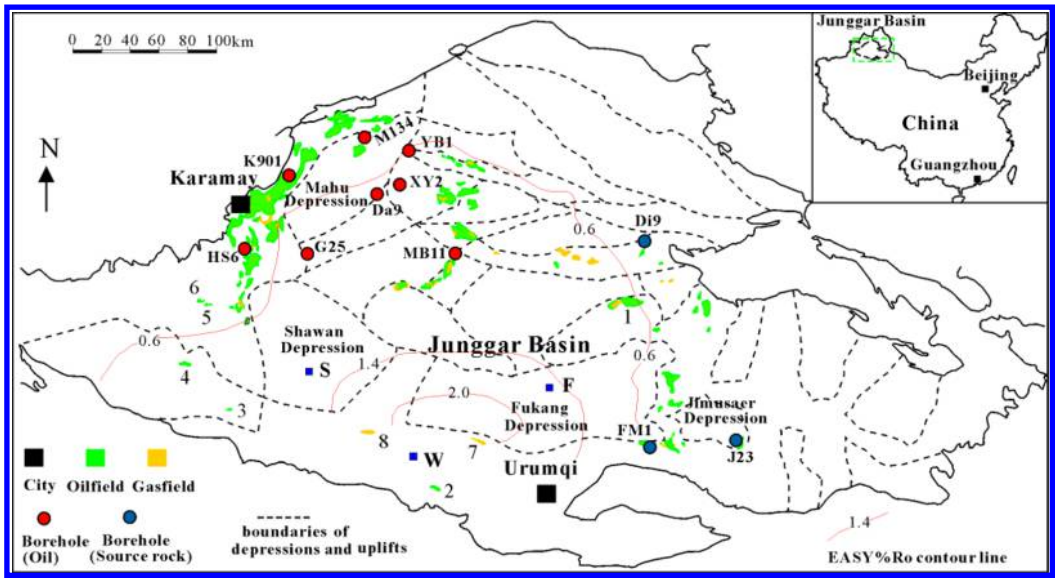

Figure 1. Location map of the Junggar Basin and sample location: (1) Cainan Oil Field; (2) Qigu Oil Field; (3) Dushanzi Oil Field; (4) Kayindike Oil Field; (5) Chunguang Oil Field; (6) Chunfeng Oil Field; (7) Hutubi Gas Field; (8) Mahe Gas Field. EASY%Ro contour lines for the bottom of the Lower Jurassic Badaowan Formation (J_{1b}) modified from Xiao et al. (2014).[27]

Hydrocarbon generation from humic coal can be simulated ideally using a confined pyrolysis system (gold capsules) as developed by Monthioux et al.[36,37] The purpose of the present study is to use programmed-temperature confined pyrolysis on two coals and one type III kerogen sample from Jurassic strata in the Junggar Basin to (1) reveal the link between gross parameters, such as H/C atomic ratio and HI value, and the yields of liquid components and gaseous hydrocarbons, (2) characterize the heterogeneity of these humic coals and terrigenous kerogen in compositions and structures, (3) obtain kinetic parameters for oil and gas generation, and (4) model hydrocarbon generation from the Jurassic coals and coaly source rocks in the southern Junggar Basin. In addition, solid state ^{13}C NMR spectroscopy has been widely used to characterize kerogen structure and composition.[38−46] In the present study, NMR spectra were used to demonstrate the relative concentrations of aliphatic carbon and aromatic carbon, and methyl ($-CH_3$) and methylene ($-CH_2-$) structural units of the coal and kerogen samples prior to heating.

2. SAMPLES AND EXPERIMENTAL DETAILS

2.1. Samples. Coals and coaly rocks are mainly found within the Lower Jurassic Badaowan Formation (J_{1b}) and Middle Jurassic Xishanyao Formation (J_{2x}) in the Junggar Basin.[47] Both formations consist of mainly sandstones, siltstones, mudstones, and coals, which were deposited in fluvial, marshy, and shallow lacustrine environments.[47] In the present study, two coals, J23C1 and FM1C2, were collected within the Middle Jurassic Xishanyao Formation (J_{2x}) from borehole J23 and within the Lower Jurassic Badaowan Formation (J_{1b}) from borehole FM1, respectively. One mudstone Di9S1 was collected within the Lower Jurassic Badaowan Formation (J_{1b}) from borehole Di9 (Figure 1). Strata columns of the Badaowan Formation (J_{1b}) in boreholes FM1 and Di9 and Xishanyao Formation (J_{2x}) in borehole J23 are demonstrated in Figure 2. The gross geochemical parameters of these samples are demonstrated in Table 1. Rock-Eval T_{max} and PI parameters of these samples range 428−439 °C and 0.03−0.04, respectively, demonstrating low maturities. Vitrinite maturation modeling (EASY%Ro)[48] for the bottom of Lower Jurassic Badaowan Formation (J_{1b}), integrating burial history and thermal gradient data,[49,50] indicates that these samples are outside the oil generation window with EASY%Ro < 0.6 (Figure 1).[27,51] Jurassic coaly source rocks in the basin contain mainly type III kerogen with bulk geochemical parameters varying substantially.[24,47,51] Samples FM1C1 and Di9S1 with relatively higher HI were selected because they are potential source rocks for both oil and gas reservoirs, while sample J23C1 with an averaged or relatively lower HI was selected because it is a typical gas-prone source rock.[3]

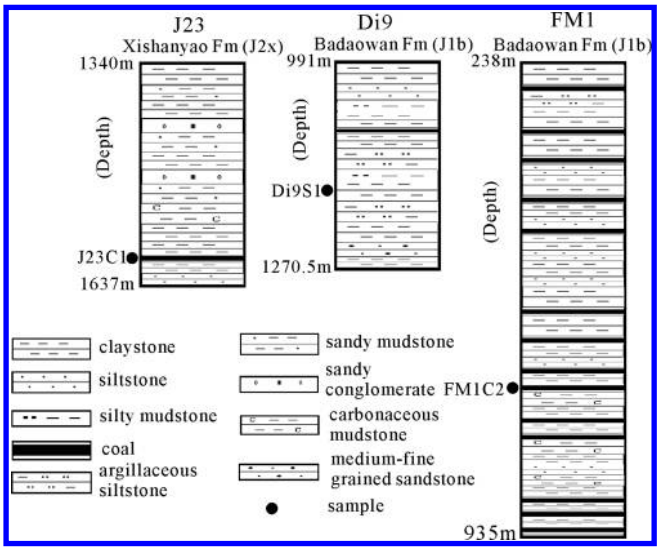

Figure 2. Strata columns for the Middle Jurassic Xishanyao Fomation (J_{2x}) in borehole J23 and Lower Jurassic Badaowan Formation (J_{1b}) in boreholes Di9 and FM1.

The coals and mudstone were ground into powder (about 200 mesh). The powder sample of Di9S1 was Soxhlet extracted with DCM:MeOH (93:7, v:v) for 72 h to remove bitumen. The extracted residue was treated with HCl and HF to obtain kerogen, as described previously.[52] However, the resultant kerogen sample is impure with carbon content 30.63% (Table 1). In the present study, the impure kerogen samples were used for the kinetical experiments assuming that further treatments with HCl and HF might lead to loss of organic matter and modification of the kerogen composition.

2.2. Solid State ^{13}C NMR Spectroscopy. The experiments were performed in a Bruker AVANCE III 400 MHz NMR spectrometer with a DP/ MAS solid double resonance probe head. Coal and

DOI: 10.1021/acs.energyfuels.6b01143
Energy Fuels 2017, 31, 73−94

Table 1. Gross Geochemical Parameters of Source Rocks[a]

	depth (m)	strata	TOC %	S1	S2	PI	HI	T_{max}	H/C	O/C	kerogen C %
J23C1	1611.5	J_{2x}	68.79	1.92	57.44	0.032	83	428	0.70	0.15	
FM1C2	711.4	J_{1b}	71.48	6.52	140.69	0.044	197	439	0.86	0.11	
DI9S1	1175.4	J_{1b}	5.26	0.45	11.87	0.037	226	436	1.01	0.15	30.63

[a]S1 and S2: in "mg/g rock"; PI = S1/(S1+S2); HI: in "mg/g TOC"; Tmax: in "°C".

Table 2. Carbon Functionalities and Relative Intensities of Corresponding Lines in ^{13}C DP MAS-NMR Spectra[a]

		J23C1		FM1C2		DI9S1	
peak no.	carbon functionality	chem shift (ppm)	area (%)	chem shift (ppm)	area (%)	chem shift (ppm)	area (%)
1	alip methyl	12.10	0.81	11.79	4.09	13.94	4.07
2	aro methyl	18.68	2.94	20.37	9.28	20.98	6.24
3	cyclic and acyclic methylene	27.87	4.33	29.25	8.10	29.40	15.89
4	aro methylene	34.92	0.90	35.22	3.08	36.45	2.52
5	methine	39.20	1.10	40.12	3.94	40.89	3.50
6	quaternary and bridgehead	45.64	1.20	45.64	2.32	46.40	2.36
7	methoxy	51.61	0.61	52.37	2.66	53.60	3.13
8	ortho-oxyaromatic	105.36	2.04	107.04	4.05	106.74	2.65
9	protonated aromatic	126.49	69.21	126.95	41.50	126.65	41.86
10	aromatic branched	142.27	5.53	140.74	5.65	140.28	5.42
11	oxy-aromatic	150.38	5.16	151.91	11.98	151.61	9.11
12	carboxy	158.50	3.89	164.62	1.64	163.25	1.79
13	carbonyl	179.94	2.27	180.40	1.70	180.55	1.48
	R1		0.145		0.530		0.639
	R2		0.717		1.20		0.560

[a]R1 = aliphatic carbon/aromatic carbon = ∑(peak 1−7)/∑(peak 8−11); R2 = methyl/methylene = ∑(peak 1−2)/∑(peak 3−4).

kerogen powder samples were first dried in a vacuum at 330 K for 12 h. About 200 mg of coal or kerogen powder was placed in a zirconia rotor. The spinning angle was adjusted to the magic angle on a standard test sample of glycine for chemical shift calibration. The magic-angle spinning speed was 14 ± 0.003 kHz, and the ^{13}C resonance frequency was 100.613 MHz. The width of 90° pulse for hydrogen spin locking was 4 μs. The recycle delay time was 25 s. Acquisition time 5.17 μs and spectral width 100 kHz were employed. Each spectrum was repeated 1000 times. The spectra were processed using software Bruker Topspin 2.1. Spectra deconvolution was performed using peak-fitting software PeakFit V.4.12 developed by SeaSolve Software Inc. The simulation procedure was repeated several times until the best fit was obtained between the simulated and experimental spectra. The final structure unit distributions and NMR spectra of coals J23C1 and FM1C2 and kerogen Di9S1 are given in Table 2 and Figure 3.

2.3. Confined Pyrolysis Experiments. Pyrolysis experiments on coal and kerogen samples were conducted in flexible gold capsules (4 mm o.d., 0.25 mm wall thickness, and 40 mm length) contained within steel pressure vessels. Each capsule was loaded with 9.66−48.78 mg of powder sample (Table 3). Three capsules containing coals J23C1 and FM1C2 and kerogen Di9S1, respectively, were placed together in each vessel. The internal pressure of the vessels, connected to each other with tubing, was adjusted to and maintained at 50 MPa by pumping water into or out of the vessels during the pyrolysis experiments. The error of the pressure is <±0.1 MPa. Our experimental system permits 14 pressure vessels to be placed in a single furnace. The performances of sample loading and pyrolysis apparatus have been described previously.[53−55]

Two heating programs were used for the pyrolysis experiments: 2 and 20 °C/h. The vessels were heated to 250 °C within 10 h, and then, from 250 to 600 °C at a rate of 2 or 20 °C/h. Two thermocouples were used to measure the temperature of the pyrolysis experiments and to check each other. The error of the recorded temperatures is < ±1 °C. Vessels containing gold capsules were removed from the oven at temperature intervals of 12 or 24 °C between 333 °C and the final temperature. Each vessel was quenched to room temperature in cold water within 10 min.

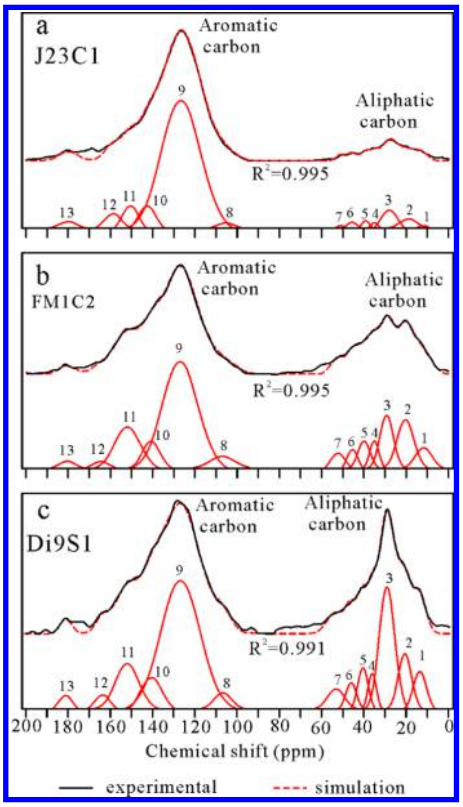

Figure 3. Structure unit distributions and ^{13}C NMR spectra of coals J23C1 and FM1C2 and kerogen Di9S1. 1−13: See Table 2.

2.4. Analysis of Gas Components. After pyrolysis, the volatile components in the capsules were collected in a special sampling device connected to an Agilent 6890N GC modified by Wasson ECE Instrumentation, as described previously.[52−56] Briefly, the whole

DOI: 10.1021/acs.energyfuels.6b01143
Energy Fuels 2017, 31, 73−94

Table 3. Measured Amounts of Bitumen, Total *n*-Alkanes ($\sum nC_{8+}$), Total Liquid Components ($\sum C_{8+}$), Oil and Gas Components Produced During Kerogen Pyrolysis Experiments (mg/g TOC)[a]

T (°C)	EASY%R_o	sample (mg)	bit	$\sum nC_{8+}$	$\sum C_{8+}$	aro	oil	A/S	C_1	C_2H_6	$C_2H_4\times10^{-3}$	C_3H_8	$C_3H_6\times10^{-3}$	iC_4	nC_4	iC_5	nC_5	$\sum C_{1-5}$	$C_1/\sum C_{1-5}$ (wt)
J23C1 (J_{2x}), 20 °C/h																			
333.3	0.56	47.56	3.06	1.71	6.66	0.65	9.99	0.34	0.21	0.027	0.809	0.019	0.212	0.0053	0.0022	0.0017	0.0014	0.27	0.789
345.5	0.61	47.89	10.62	1.91	7.01	0.72	10.52	0.38	0.26	0.036	1.144	0.021	0.213	0.0075	0.0029	0.0021	0.0015	0.34	0.783
369.7	0.72	43.06	11.82	3.34	13.87	1.08	20.81	0.41	0.56	0.131	0.812	0.064	0.391	0.0161	0.0051	0.0037	0.0017	0.78	0.715
381.6	0.78	42.09	12.43	5.14	17.82	1.18	26.73	0.42	0.88	0.269	0.914	0.112	0.514	0.0181	0.0096	0.0043	0.0026	1.30	0.679
393.8	0.85	40.81	16.03	7.15	23.62	1.90	35.44	0.40	1.44	0.584	1.029	0.260	0.677	0.0323	0.0238	0.0072	0.0048	2.36	0.612
406.1	0.94	38.45	15.50	9.07	29.07	2.09	43.60	0.39	2.21	0.985	2.032	0.404	2.062	0.0526	0.0388	0.0108	0.0072	3.71	0.596
418.8	1.05	37.80	17.69	10.49	32.82	2.25	49.23	0.38	3.01	1.323	1.511	0.522	1.653	0.0660	0.0553	0.0137	0.0106	5.01	0.602
430.7	1.18	35.69	12.63	11.04	35.36	3.36	53.05	0.40	4.28	1.881	2.287	0.712	2.390	0.0809	0.0812	0.0170	0.0158	7.08	0.605
442.7	1.31	34.14	12.35	11.52	39.60	3.68	59.37	0.43	5.40	2.368	2.493	0.893	3.343	0.0886	0.1076	0.0185	0.0205	8.90	0.607
466.8	1.62	30.17	7.71	4.87	34.34	6.29	51.52	0.72	10.79	4.094	4.251	1.293	6.770	0.0873	0.1516	0.0131	0.0213	16.46	0.655
478.6	1.79	28.72	7.59	1.77	31.81	6.72	47.72	0.91	13.88	4.660	7.714	1.230	15.060	0.0668	0.1307	0.0082	0.0148	20.02	0.694
490.2	1.97	26.28	6.64	0.32	31.27	8.94	46.92	0.99	17.63	5.273	6.655	1.159	10.972	0.0505	0.1006	0.0043	0.0083	24.24	0.727
502.1	2.16	24.73							21.82	5.377	7.072	0.775	7.773	0.0285	0.0420	0.0017	0.0027	28.06	0.778
514.2	2.37	22.43							28.07	5.181	8.317	0.524	5.356	0.0149	0.0154	0.0008	0.0013	33.82	0.830
526.0	2.58	21.08							33.66	4.611	7.191	0.292	2.394	0.0066	0.0039	0.0007	0.0010	38.58	0.872
537.6	2.79	19.03							37.93	3.065	5.392	0.076	0.499	0.0017	0.0014	0.0007	0.0008	41.08	0.923
549.8	3.02	17.32							46.30	1.864	2.558	0.020	0.000	0.0007	0.0011	0.0010	0.0008	48.19	0.961
574.1	3.46	13.81							52.23	0.825	0.000	0.007	0.000	0.0007	0.0013	0.0008	0.0008	53.06	0.984
588.6	3.70	11.88							58.69	0.780	0.000	0.007	0.000	0.0000	0.0000	0.0008	0.0011	59.48	0.987
597.8	3.84	10.01							60.72	0.714	0.000	0.006	0.000	0.0000	0.0000	0.0000	0.0000	61.44	0.988
J23C1 (J_{2x}), 2 °C/h																			
334.9	0.72	45.02	14.53	3.51	11.44	0.63	17.16	0.42	0.53	0.111	0.337	0.052	0.000	0.0136	0.0033	0.0028	0.0009	0.72	0.744
346.8	0.78	43.79	11.29	4.96	15.80	0.73	23.70	0.43	0.82	0.229	0.825	0.095	0.000	0.0169	0.0066	0.0031	0.0016	1.17	0.699
371.0	0.95	40.49	11.85	9.52	28.96	2.28	43.45	0.40	1.96	0.810	0.518	0.316	0.712	0.0399	0.0277	0.0075	0.0054	3.16	0.618
382.9	1.07	39.51	12.14	11.92	36.40	2.82	54.61	0.42	3.11	1.325	0.797	0.443	0.578	0.0579	0.0427	0.0103	0.0073	5.00	0.622
395.1	1.21	36.73	19.00	11.45	37.28	3.46	55.92	0.42	5.15	2.214	1.302	0.738	1.014	0.0635	0.0742	0.0116	0.0125	8.27	0.623
407.6	1.35	35.32	10.70	9.28	37.29	4.58	55.94	0.55	7.73	3.066	1.023	0.895	1.599	0.0566	0.0974	0.0102	0.0140	11.87	0.651
419.8	1.51	34.28	8.06	3.85	27.36	5.01	41.04	0.71	10.94	3.896	3.231	0.995	5.608	0.0556	0.0964	0.0079	0.0107	16.01	0.683
431.5	1.68	32.47	13.43	2.02	26.99	5.33	40.49	0.86	13.72	4.843	2.945	1.302	5.550	0.0444	0.0865	0.0055	0.0087	20.01	0.685
441.8	1.85	31.00	8.44	0.44	23.48	6.61	35.23	0.98	17.16	4.831	3.197	0.901	3.876	0.0387	0.0667	0.0035	0.0048	23.01	0.746
467.6	2.29	27.67	9.98	0.00	24.49	9.07	36.74	1.00	29.33	4.355	3.203	0.270	1.303	0.0071	0.0067	0.0003	0.0007	33.98	0.863
479.4	2.51	25.69							35.25	3.739	2.950	0.127	0.982	0.0027	0.0018	0.0002	0.0006	39.13	0.901
490.9	2.73	24.43							40.46	2.298	0.000	0.030	0.000	0.0005	0.0007	0.0000	0.0000	42.79	0.946
502.9	2.97	23.24							43.99	1.643	0.000	0.015	0.000	0.0003	0.0008	0.0000	0.0000	45.65	0.964
514.9	3.21	21.70							51.13	0.942	0.000	0.011	0.000	0.0000	0.0000	0.0000	0.0000	52.09	0.982
526.5	3.43	19.59							55.58	0.772	0.000	0.007	0.000	0.0000	0.0000	0.0000	0.0000	56.36	0.986
538.7	3.65	18.02							60.80	0.679	0.000	0.006	0.000	0.0000	0.0000	0.0000	0.0000	61.48	0.989
551.6	3.86	16.27							64.42	0.562	0.000	0.005	0.000	0.0000	0.0000	0.0000	0.0000	64.99	0.991
574.7	4.17	13.06							80.23	0.498	0.000	0.003	0.000	0.0000	0.0000	0.0000	0.0000	80.73	0.994
586.8	4.31	11.35							85.45	0.469	0.000	0.003	0.000	0.0000	0.0000	0.0000	0.0000	85.92	0.995

DOI: 10.1021/acs.energyfuels.6b01143
Energy Fuels 2017, 31, 73−94

Table 3. continued

T (°C)	EASY%R_o	sample (mg)	bit	$\sum nC_{8+}$	$\sum C_{8+}$	aro	oil	A/S	C_1	C_2H_6	$C_2H_4\times10^{-3}$	C_3H_8	$C_3H_6\times10^{-3}$	iC_4	nC_4	iC_5	nC_5	$\sum C_{1-5}$	$C_1/\sum C_{1-5}$ (wt)
J23C1 (J_{2x}), 2 °C/h																			
598.6	4.43	10.44							90.32	0.370	0.000	0.000	0.000	0.0000	0.0000	0.0000	0.0000	90.69	0.996
FM1C2 (J_{1b}), 20 °C/h																			
333.3	0.56	48.71	9.19	2.78	20.08	0.99	30.12	0.56	0.07	0.006	0.599	0.002	0.38	0.0078	0.0002	0.0002	0.0001	0.09	0.800
345.5	0.61	46.90	4.18	2.97	20.08	2.03	30.13	0.52	0.10	0.010	0.502	0.002	0.39	0.0095	0.0005	0.0003	0.0002	0.13	0.817
369.7	0.72	42.07	11.97	3.94	25.85	0.89	38.78	0.59	0.60	0.107	0.987	0.027	0.66	0.0259	0.0029	0.0046	0.0006	0.77	0.779
381.6	0.78	40.68	33.70	6.01	37.46	2.31	56.20	0.54	1.54	0.447	1.324	0.130	1.65	0.0522	0.0126	0.0091	0.0018	2.19	0.701
393.8	0.85	40.65	30.28	8.75	49.29	3.92	73.95	0.54	3.01	1.651	2.043	0.842	5.12	0.1315	0.1127	0.0339	0.0166	5.80	0.518
406.1	0.94	39.31	58.01	17.01	82.63	4.98	123.96	0.44	6.29	3.511	4.852	1.497	9.41	0.2635	0.1906	0.0477	0.0264	11.84	0.531
418.8	1.05	36.35	78.51	19.19	89.62	2.83	134.45	0.42	9.86	6.091	7.408	3.048	17.49	0.5427	0.4626	0.1160	0.0672	20.21	0.488
430.7	1.18	35.41	64.00	23.56	110.70	3.64	166.06	0.39	13.59	8.634	9.506	4.942	26.12	0.9464	0.9385	0.2577	0.1588	29.50	0.461
442.7	1.31	32.83	75.85	23.11	109.15	3.01	163.74	0.41	17.94	11.315	11.962	7.012	37.33	1.3708	1.5997	0.4740	0.3267	40.09	0.448
466.8	1.62	29.65	26.89	16.67	93.19	9.59	139.80	0.56	31.58	16.905	16.273	10.496	55.37	1.9384	2.6315	0.7010	0.5857	64.91	0.487
478.6	1.79	27.81	27.16	5.89	78.16	7.50	117.25	0.79	38.86	19.470	21.787	11.740	75.66	2.0974	2.7729	0.6511	0.5339	76.22	0.510
490.2	1.97	25.90	49.15	1.19	72.57	8.64	108.87	0.96	46.20	21.226	22.528	11.881	77.22	2.1126	2.3491	0.5163	0.3305	84.72	0.545
502.1	2.16	24.21							58.90	22.942	23.173	10.415	62.08	2.0306	1.2763	0.3084	0.0908	96.05	0.613
514.2	2.37	22.51							68.96	23.203	26.419	7.629	53.93	1.5746	0.5234	0.0992	0.0201	102.09	0.675
526.0	2.58	20.35							81.95	22.290	25.915	5.447	38.63	1.2054	0.1491	0.0309	0.0045	111.14	0.737
537.6	2.79	19.38							92.69	18.321	24.896	2.509	23.86	0.3217	0.0281	0.0062	0.0028	113.93	0.814
549.8	3.02	17.26							110.44	12.894	23.403	0.578	8.04	0.0638	0.0071	0.0026	0.0017	124.02	0.891
574.1	3.46	13.27							129.20	4.758	10.992	0.048	1.48	0.0049	0.0034	0.0017	0.0013	134.03	0.964
588.6	3.70	11.88							137.87	2.490	11.334	0.024	1.27	0.0039	0.0030	0.0016	0.0013	140.40	0.982
597.8	3.84	9.66							144.49	1.757	5.575	0.017	0.00	0.0036	0.0024	0.0013	0.0015	146.28	0.988
FM1C2 (J_{1b}), 2 °C/h																			
334.9	0.72	45.05	30.12	4.67	31.61	1.91	47.42	0.59	0.56	0.096	0.548	0.026	0.38	0.0249	0.0030	0.0043	0.0007	0.71	0.781
346.8	0.78	43.17	25.92	5.64	34.21	2.08	51.32	0.55	1.32	0.346	0.884	0.099	0.70	0.0399	0.0093	0.0070	0.0014	1.82	0.723
371.0	0.95	40.02	61.52	16.19	87.89	4.50	131.85	0.48	5.70	3.234	2.383	1.464	3.47	0.2780	0.1761	0.0498	0.0224	10.93	0.521
382.9	1.07	38.46	72.38	24.93	117.10	8.87	175.57	0.41	9.17	5.936	3.793	3.107	6.91	0.5208	0.4508	0.1034	0.0603	19.36	0.474
407.6	1.35	35.60	33.79	26.10	117.22	10.33	175.75	0.43	21.68	12.760	6.619	7.910	14.94	1.4639	1.7412	0.5028	0.3392	46.42	0.467
419.8	1.51	33.99	32.92	20.73	104.19	7.34	156.30	0.51	28.65	15.295	7.593	9.233	17.35	1.7014	2.0562	0.6344	0.4108	58.00	0.494
431.5	1.68	32.63	47.59	13.72	90.31	6.65	135.48	0.58	33.64	17.091	8.941	10.073	20.20	2.3810	2.3479	1.2071	0.5637	67.33	0.500
441.8	1.85	30.82	21.33	4.84	82.54	9.34	123.83	0.90	45.02	20.109	10.558	10.819	24.38	2.4040	2.0996	0.9046	0.3552	81.74	0.551
467.6	2.29	27.24	26.70	0.00	44.03	8.56	66.06	1.00	69.68	22.344	12.357	7.608	18.25	2.1356	0.7398	0.2570	0.0491	102.84	0.678
479.4	2.51	26.29							81.38	19.797	12.804	4.135	13.19	1.0954	0.1581	0.0379	0.0076	106.64	0.763
490.9	2.73	24.61							95.18	17.297	11.854	1.951	6.58	0.4471	0.0271	0.0079	0.0029	114.94	0.828
502.9	2.97	22.83							106.29	12.406	10.321	0.585	2.48	0.1139	0.0073	0.0038	0.0021	119.42	0.890
526.5	3.43	19.60							126.25	4.201	6.870	0.049	1.36	0.0062	0.0035	0.0027	0.0018	130.53	0.967
538.7	3.65	17.51							135.49	1.887	0.000	0.026	0.00	0.0045	0.0031	0.0024	0.0018	137.42	0.986
551.6	3.86	16.54							139.33	1.032	0.000	0.014	0.00	0.0028	0.0017	0.0016	0.0013	140.38	0.992
574.7	4.17	12.19							151.53	0.680	0.000	0.009	0.00	0.0028	0.0019	0.0021	0.0011	152.22	0.995
586.8	4.31	12.73							155.32	0.575	0.000	0.008	0.00	0.0022	0.0015	0.0014	0.0012	155.91	0.996
598.6	4.43	10.28							156.73	0.494	0.000	0.007	0.00	0.0024	0.0019	0.0000	0.0000	157.24	0.997

DOI: 10.1021/acs.energyfuels.6b01143
Energy Fuels 2017, 31, 73−94

Table 3. continued

T (°C)	EASY%R_o	sample (mg)	bit	$\sum nC_{8+}$	$\sum C_{8+}$	aro	oil	A/S	C_1	C_2H_6	$C_2H_4\times10^{-3}$	C_3H_8	$C_3H_6\times10^{-3}$	iC_4	nC_4	iC_5	nC_5	$\sum C_{1-5}$	$C_1/\sum C_{1-5}$ (wt)
Di9S1 (J_{1b}), 20 °C/h																			
333.3	0.56	48.78	8.70	0.91	11.42	1.65	17.14	0.68	0.46	0.253	1.879	0.242	4.09	0.2153	0.0420	0.0606	0.0100	1.28	0.355
345.5	0.61	47.18	8.99	1.21	13.17	1.80	19.75	0.70	0.67	0.461	2.053	0.493	5.60	0.3771	0.0869	0.1168	0.0202	2.23	0.301
369.7	0.72	43.38	24.08	3.43	22.26	3.00	33.40	0.64	1.73	1.658	2.656	1.810	8.08	0.9554	0.3492	0.3521	0.0772	6.94	0.249
381.6	0.78	41.56	30.63	4.20	33.29	4.47	49.94	0.69	2.80	2.978	3.654	3.007	6.49	1.2943	0.5922	0.4606	0.1191	11.26	0.249
393.8	0.85	39.29	31.57	5.45	29.32	4.49	43.98	0.57	4.70	5.113	5.398	4.779	9.61	1.8800	1.0793	0.8591	0.2664	18.69	0.251
406.1	0.94	38.03	43.77	9.40	53.86	6.35	80.75	0.56	7.26	7.630	6.885	6.487	10.64	2.2676	1.4049	1.0425	0.3179	26.43	0.275
418.8	1.05	36.48	48.32	8.17	52.57	6.81	78.86	0.57	10.14	10.029	6.603	7.896	11.09	2.5480	1.7006	1.1825	0.3844	33.90	0.299
430.7	1.18	35.26	16.66	7.67	42.54	6.96	63.81	0.57	13.58	12.028	6.015	8.692	9.95	2.6252	1.9749	1.2047	0.4554	40.58	0.335
442.7	1.31	32.36	10.09	4.77	36.65	10.55	54.99	0.61	17.97	14.403	5.906	9.722	8.34	2.7691	2.0566	1.3127	0.4445	48.69	0.369
466.8	1.62	29.12	28.02	2.68	35.88	13.95	53.83	0.79	33.82	19.297	8.991	10.866	22.23	2.8269	2.4697	1.2868	0.5506	71.15	0.475
478.6	1.79	27.94	8.18	0.60	35.80	19.65	53.71	0.96	43.17	21.281	5.876	10.825	11.68	2.7502	2.3392	1.0918	0.3994	81.87	0.527
490.2	1.97	26.65							49.87	22.189	11.789	10.666	18.22	2.4369	2.0622	0.7903	0.2776	88.32	0.565
502.1	2.16	23.26							65.48	22.211	9.680	7.565	11.60	1.1786	0.9310	0.1511	0.0499	97.59	0.671
514.2	2.37	25.34							72.70	21.854	10.332	6.475	10.65	0.7083	0.5732	0.0399	0.0122	102.39	0.710
526.0	2.58	19.82							81.00	19.858	8.587	4.987	11.57	0.4174	0.2578	0.0153	0.0057	106.56	0.760
537.6	2.79	20.33							97.17	16.085	12.235	2.182	6.77	0.1123	0.0600	0.0095	0.0037	115.64	0.840
549.8	3.02	17.68							107.59	11.742	9.182	0.743	3.51	0.0205	0.0128	0.0043	0.0022	120.13	0.896
574.1	3.46	13.92							128.54	5.263	7.147	0.213	3.49	0.0112	0.0078	0.0051	0.0024	134.05	0.959
588.6	3.70	11.26							142.75	4.121	0.000	0.134	0.00	0.0081	0.0067	0.0045	0.0020	147.02	0.971
597.8	3.84	10.27							142.87	3.417	0.000	0.123	0.00	0.0068	0.0043	0.0034	0.0030	146.43	0.976
Di9S1 (J_{1b}), 2 °C/h																			
334.9	0.72	44.72	16.06	3.08	24.43	4.10	36.65	0.67	1.03	0.953	1.581	1.101	2.41	0.7470	0.2059	0.2686	0.0496	4.36	0.236
346.8	0.78	43.42	32.16	4.95	33.37	5.17	50.06	0.72	2.35	2.583	2.774	2.772	3.85	1.3708	0.5041	0.4531	0.0997	10.14	0.232
371.0	0.95	40.60	16.54	7.75	38.85	6.05	58.28	0.61	6.16	6.996	4.450	6.107	4.25	2.2792	1.2163	0.9510	0.2667	23.99	0.257
382.9	1.07	38.41	23.80	7.03	43.48	6.45	65.22	0.74	10.00	10.241	4.090	7.534	4.14	2.4666	1.4713	1.0697	0.2798	33.07	0.302
395.1	1.21	37.70	12.99	4.86	53.25	17.85	79.88	0.77	15.93	13.930	2.570	9.282	3.86	2.7119	1.8306	1.1187	0.3467	45.16	0.353
407.6	1.35	35.05	17.69	2.83	50.24	24.18	75.37	0.87	23.82	16.567	1.494	9.438	4.23	2.3353	1.7507	0.8044	0.2603	54.98	0.433
419.8	1.51	33.56	9.73	2.08	47.09	23.39	70.64	0.85	32.13	18.186	3.511	8.983	6.67	2.1043	1.6948	0.7210	0.2673	64.10	0.501
431.5	1.68	32.32	4.04	1.08	40.30	17.04	60.45	0.91	39.54	19.687	4.294	8.535	7.85	2.0495	1.6900	0.6540	0.2425	72.41	0.546
441.8	1.85	30.22							48.25	19.819	5.545	7.484	5.45	1.3843	1.1492	0.2912	0.0989	78.49	0.615
467.6	2.29	27.67							74.09	17.130	3.501	3.030	4.58	0.2887	0.2071	0.0210	0.0079	94.78	0.782
479.4	2.51	26.23							88.41	14.536	4.392	2.004	3.60	0.1839	0.1127	0.0106	0.0041	105.27	0.840
490.9	2.73	24.24							97.62	11.325	4.645	1.101	2.45	0.0674	0.0407	0.0055	0.0029	110.17	0.886
502.9	2.97	22.96							112.50	6.693	0.000	0.353	0.00	0.0158	0.0108	0.0052	0.0028	119.58	0.941
514.9	3.21	20.79							116.98	4.679	0.000	0.358	0.00	0.0087	0.0057	0.0033	0.0017	122.03	0.959
526.5	3.43	20.29							130.42	3.569	0.000	0.238	0.00	0.0065	0.0043	0.0026	0.0013	134.24	0.972
538.7	3.65	18.94							138.06	2.773	0.000	0.107	0.00	0.0041	0.0025	0.0016	0.0012	140.95	0.980
551.6	3.86	16.25							155.50	2.350	0.000	0.074	0.00	0.0037	0.0027	0.0020	0.0025	157.93	0.985
574.7	4.17	12.84							178.21	1.120	0.000	0.041	0.00	0.0028	0.0038	0.0032	0.0020	179.39	0.993
586.8	4.31	11.27							197.18	0.947	0.000	0.027	0.00	0.0000	0.0000	0.0000	0.0000	198.15	0.995
598.6	4.43	10.39							196.46	0.737	0.000	0.019	0.00	0.0000	0.0000	0.0000	0.0000	197.22	0.996

DOI: 10.1021/acs.energyfuels.6b01143
Energy Fuels 2017, 31, 73−94

Table 3. continued

[a]The following abbreviations apply: bit, bitumen (mg/g TOC); aro, toluene + ethylbenzene + xylenes (mg/g TOC); A/S, aromatics/saturates ratio = (β- + α-methylnaphthalenes)/(β- + α-methylnaphthalenes + 2 × n-C_{13}).

device was at first evacuated to <1 × 10^{-2} Pa. The gold capsule was then pierced with a needle, allowing the gases to escape into the device. The valve connecting the device and the modified GC was open to allow the gas to enter the GC. The GC analyses of both the organic and inorganic gas components were performed in an automatically controlled procedure. The oven temperature for the hydrocarbon gas analysis was initially held at 70 °C for 6 min, ramped from 70 to 130 °C at 15 °C/min, from 130 to 180 °C at 25 °C/min, and then held at 180 °C for 4 min. A test with external standard gases ($CH_4/CO_2/C_2H_6/C_3H_8$ = 5:5:2:1, in volume) indicated that the amounts of gas products measured using this device had better than 0.5% relative error.

2.5. Analyses for Bitumen and Liquid Components. After analysis for gas components, the capsules that were heated at lower temperatures (332−502 °C) were cut swiftly into several pieces in a vial, which contained about 3 mL of pentane. Internal standard deuterated n-C_{24} ranging from 0.015 to 0.030 mg was added for each vial. Following five ultrasonic treatments of 5 min per treatment using an ultrasonic instrument with electronic power 250 W and operating frequency 40 kHz; these vials were allowed to settle for 72 h until the pentane solutions became clear. The pentane solutions (total pentane extracts) in all the vials were directly injected into an HP6890 GC fitted with a 30 m × 0.32 mm i.d. column coated with a 0.25 μm film of HP-5, employing nitrogen as carrier gas. The oven temperature was programmed as follows: 50 °C for 5 min, raised from 50 to 150 °C at 2 °C/min, and from 150 to 290 °C at 4 °C/min, and then held at 290 °C for 15 min. In order to determine the amount of oil based on the amount of liquid components measured from gas chromatograms, eight nonbiodegraded light oils from boreholes Da9, G25, HS6, K901, M134, MB11, XY2, and YB1 within and around the Mahu Depression were selected (Figure 1). These oils, ranging from 6.94 to 28.46 mg, were added to vials containing about 3 mL of pentane and internal standard deuterated n-C_{24} ranging from 0.032 to 0.061 mg. GC analysis was also performed for these diluted oils using the same procedure as the pyrolysates. The amounts of total liquid components ($\sum C_{8+}$) are in the range 505−808 mg/g oil with an averaged value of 667 mg/g oil for the eight oils. The amount of total liquid components ($\sum C_{8+}$) for each capsule of the coal and kerogen samples was divided by 0.667, the averaged value for the eight oils (667 mg/g oil), yielding the amount of oil produced during pyrolysis for each capsule.

After GC analyses, samples in these vials were filtered to separate the pentane solution and the solid residues. The solid residues were Soxhlet extracted with DCM/MeOH (93:7, v:v) for 72 h. The extracts were combined with the initial pentane soluble fraction to obtain the heavy pyrolysates (bitumen).

2.6. Kinetic Modeling for the Generation of Oil and Hydrocarbon Gases and Vitrinite Reflectance. Kinetic parameters were determined for the generation of oil and hydrocarbon gases using Kinetics 2000 software developed by Braun and Burnham.[57] At first, we set a range 1 × 10^{11} s^{-1} to 1 × 10^{18} s^{-1} for the A factor in running the Kinetics software, referenced from the previous studies.[58−60] After input of the data from the two heating rates, i.e., time, temperature, and transformation ratio for the generation of oil or gaseous hydrocarbons (methane, total gaseous hydrocarbons), a frequency factor A and a discrete distribution of activation energies were obtained.

Sweeney and Burnham[48] present a vitrinite maturation model to calculate the vitrinite reflectance %Ro, called as EASY%Ro, using an Arrhenius first-order parallel-reaction approach with a distribution of activation energies. EASY%Ro values were used as a maturity parameter to indicate thermal stress in isothermal or nonisothermal confined pyrolysis experimental studies.[55,61] In the present study, EASY%Ro was used as a maturity parameter to indicate thermal stress achieved at two heating rates, as in the previous studies.[55,61]

3. RESULTS

3.1. Amounts of Bitumen, Total n-Alkanes ($\sum n$-C_{8+}), Light Aromatics, Total Liquid Components ($\sum C_{8+}$), and Oil and Aromaticity. The C_6 and C_7 hydrocarbons were

DOI: 10.1021/acs.energyfuels.6b01143
Energy Fuels 2017, 31, 73−94

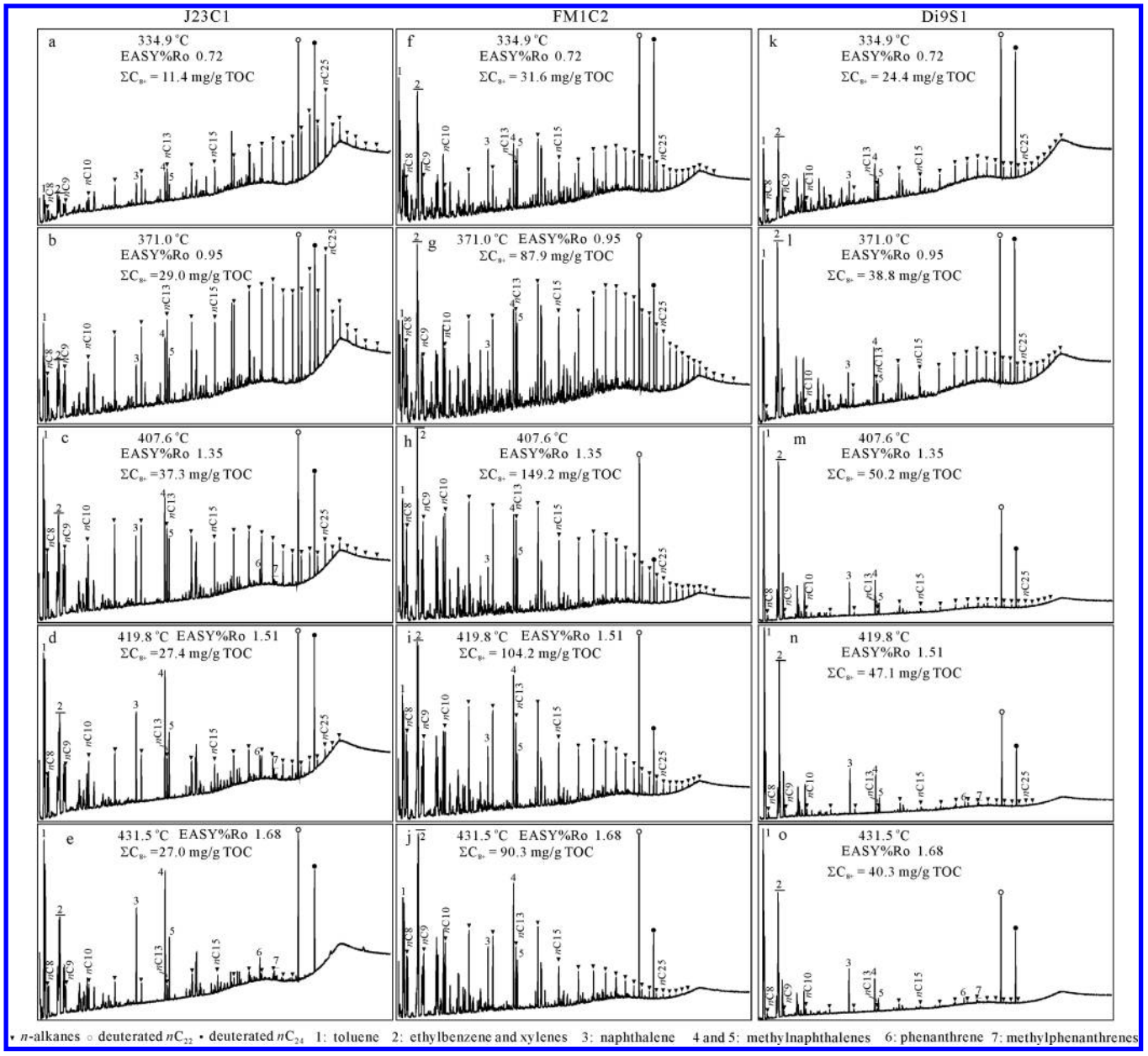

Figure 4. Selected gas chromatograms of liquid hydrocarbons from coals J23C1 and FM1C2 and kerogen Di9S1 with EASY%Ro 0.72%, 0.95%, 1.35%, 1.51%, and 1.68% at a heating rate 2 °C/h.

heavily evaporated during the analysis of gas components. Therefore, only n-C_{8+} species were measured for the amount of total n-alkanes ($\sum n$-C_{8+}), and toluene and C_{8+} components were measured for the amount of total liquid components ($\sum C_{8+}$) as shown in Table 3. The gas chromatograms of liquid hydrocarbons for selected capsules of coals J23C1 and FM1C2 and kerogen Di9S1 from 334.9 to 431.5 °C at 2 °C/h experiment are shown in Figure 4.

The amounts of bitumen, total n-alkanes ($\sum n$-C_{8+}), total liquid components ($\sum C_{8+}$), light aromatics (toluene, ethylbenzene, and xylenes), and oil and ratio of methylnaphthalenes/(methylnaphthalenes + 2 × n-C_{13}) for capsules at lower temperatures are shown in Table 3 and Figure 5.

The amounts of bitumen, total n-alkanes ($\sum n$-C_{8+}), total liquid components ($\sum C_{8+}$), and oil generally increase at first, and then decrease (Table 3 and Figure 5a–c). The total amount of toluene, ethylbenzene, and xylenes increases consistently with temperature and EASY%Ro value for coal J23C1 at both heating rates and coal FM1C2 and kerogen Di9S1 at 20 °C/h while it at first increases to a maximum at EASY%Ro 1.35, and then decreases for coal FM1C2 and kerogen Di9S1 at 2 °C/h (Table 3 and Figure 5d). The total amount of light monoaromatic components is strikingly different for kerogen Di9S1 between the two heating rates at EASY%Ro 1.35–1.51 (Table 3 and Figure 5d).

The ratio of methylnaphthalenes/(methylnaphthalenes + 2 × n-C_{13}) varies irregularly at EASY%Ro < 1.31, and then increases consistently up to 1.0 for three samples at both heating rates (Table 3 and Figure 5e). This ratio is similar for coals J23C1 and FM1C2 between the two heating rates but differ substantially for kerogen Di9S1 between the two heating rates at EASY%Ro 1.0–1.6 (Table 3 and Figure 5e).

3.2. Amounts of Gaseous Hydrocarbons and $C_1/\sum C_{1-5}$ Ratio. The amounts of gaseous hydrocarbons and the C_1/

DOI: 10.1021/acs.energyfuels.6b01143
Energy Fuels 2017, 31, 73–94

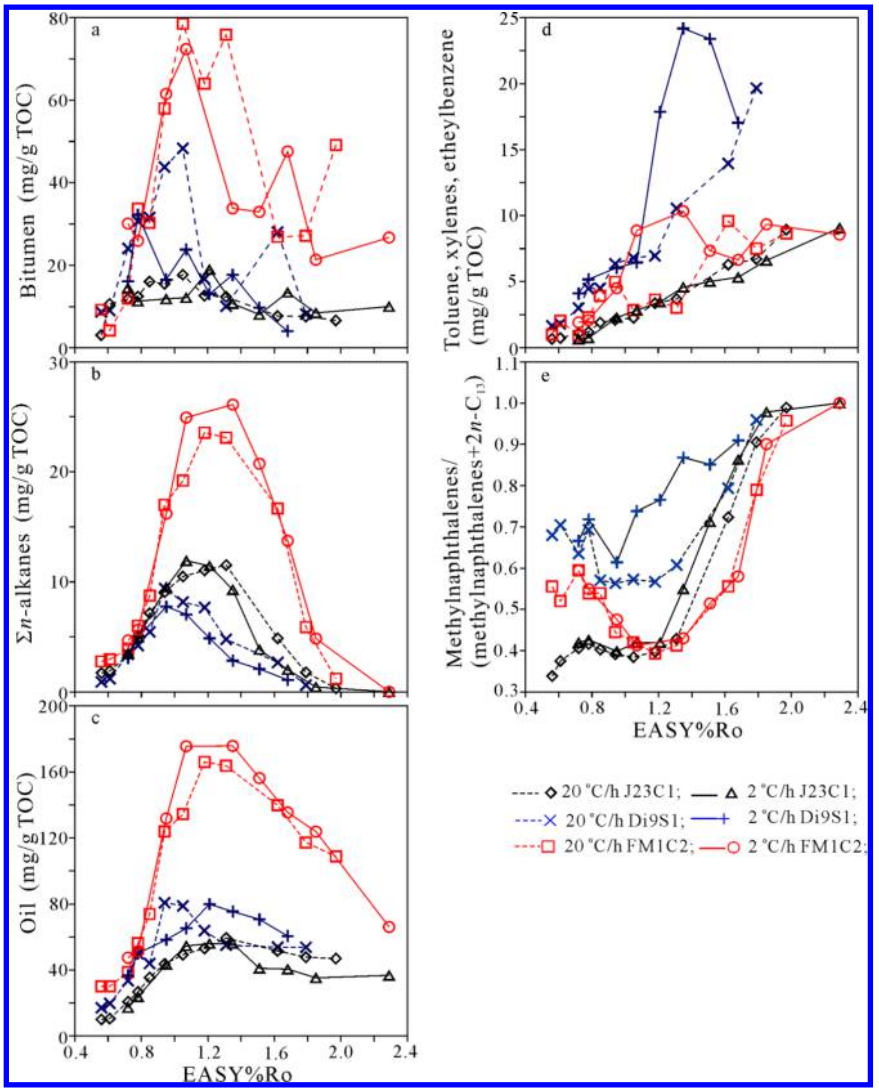

Figure 5. Measured amounts of bitumen, total *n*-alkanes ($\sum n$-C_{8+}), total liquid components ($\sum C_{8+}$), oil, and light aromatics (toluene, ethylbenzene, and xylenes) and methylnaphthalenes/(methylnaphthalenes + 2 × *n*-C_{13}) ratio versus vitrinite reflectance (EASY%Ro): (a) bitumen, (b) $\sum n$-C_{8+}, (c) oil, (d) light aromatics (toluene, ethylbenzene and xylenes), and (e) methylnaphthalenes/(methylnaphthalenes + 2 × *n*-C_{13}) ratio.

$\sum C_{1-5}$ ratio are shown in Table 3 and Figure 6. For all coal and kerogen samples, the amounts of methane and total gaseous hydrocarbons generally increase consistently with temperature and EASY%Ro at the two heating rates (Figure 6a,g).

With temperature and EASY%Ro increasing, for all the coal and kerogen samples at both heating rates, the amounts of ethane, propane, butanes, pentanes, and the total wet gases ($\sum C_{2-5}$) at first increase to maximum values, and then decrease (Figure 6b–f). For coals J23C1 and FM1C2, the amounts of individual wet gas and the total are generally similar between the two heating rates at a same EASY%Ro. However, for kerogen Di9S1, the amounts of individual wet gas and the total are similar between the two heating rates at lower EASY%Ro, but decrease earlier and are significantly lower at 2 than at 20 °C/h at higher EASY%Ro (Figure 6b–f).

For all three samples, the $C_1/\sum C_{1-5}$ ratio at first decreases to the lowest value and then increases consistently toward 1.0 (Figure 6h). For coals J23C1 and FM1C2, this ratio is similar between the two heating rates, but for kerogen Di9S1, it is relatively higher at 2 than at 20 °C/h at EASY%Ro > 1.2 (Figure 6h).

4. DISCUSSION

4.1. Relationship between Parameters HI and H/C Ratio and the Yields of Liquid and Gaseous Hydrocarbons. Kerogen Di9S1 has the highest Rock-Eval hydrogen index (HI) and H/C atomic ratio; however, it has the lowest maximum yield of total *n*-alkanes ($\sum n$-C_{8+}) among the three samples (Tables 1 and 3, and Figure 5b). The maximum yields of total *n*-alkanes and oil are substantially higher for coal FM1C2 than kerogen Di9S1 although the former has a lower HI value and H/C atomic ratio than the latter (Table 3 and Figures 4 and 5). Isaksen et al.[19] suggested that the main control on the oil potential is the concentration of long-chain aliphatic hydrocarbons in the coal matrix, and the HI value is a poor indicator of the nonvolatile oil potential of humic coals. Previous studies also suggested that the generative potential of coals is commonly overestimated by Rock-Eval pyrolysis because coals generate higher amounts of volatile mono-aromatic hydrocarbons and phenols upon open pyrolysis which do not contribute to the nonvolatile oil generation potential of the organic matter.[18,19,62]

DOI: 10.1021/acs.energyfuels.6b01143
Energy Fuels 2017, 31, 73–94

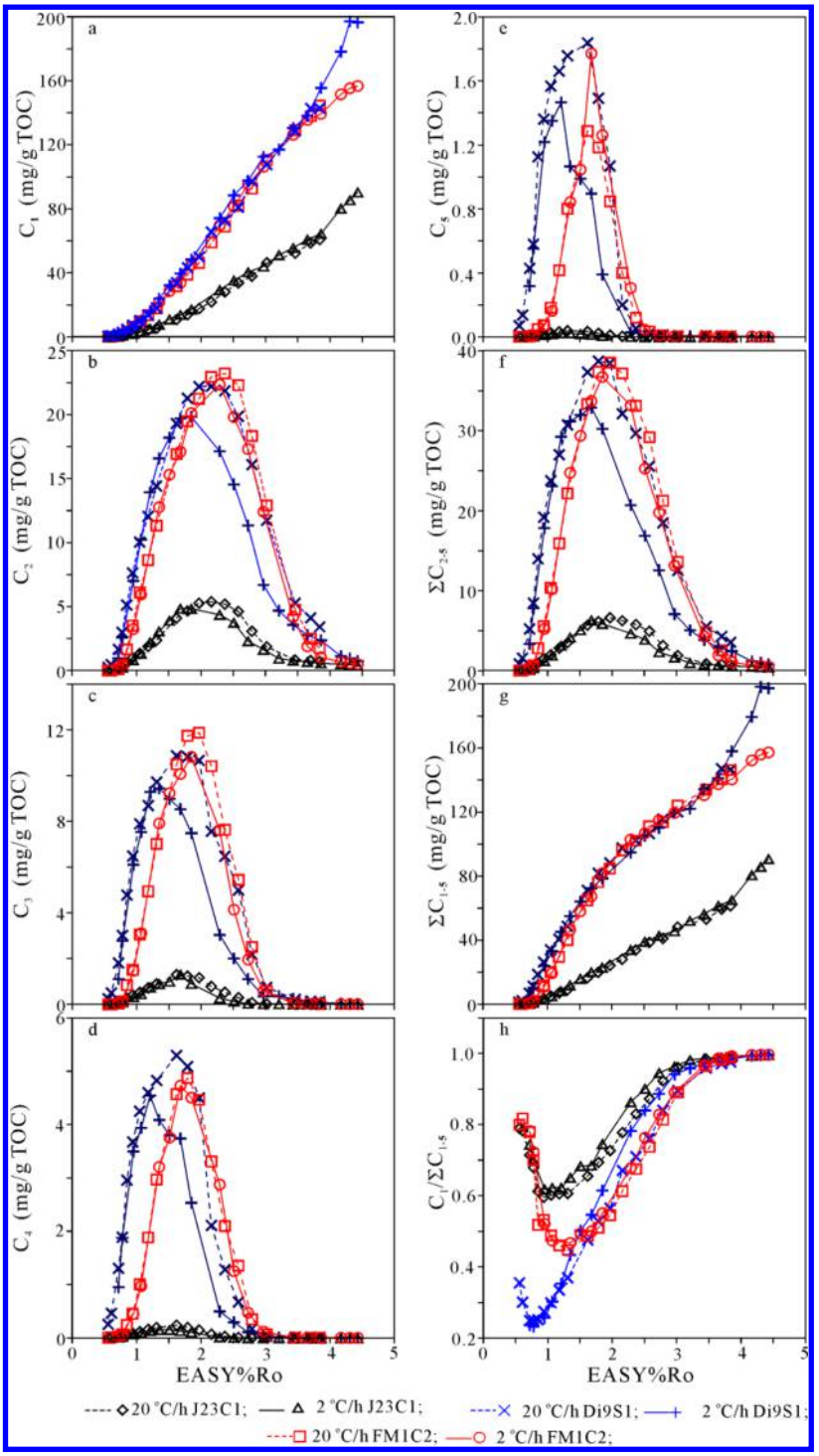

Figure 6. Measured amounts of gaseous hydrocarbons and $C_1/\sum C_{1-5}$ ratio versus vitrinite reflectance (EASY%Ro).

The yields of methane and total gaseous hydrocarbons at the highest temperature and maturity increase from coal J23C1, through coal FM1C2 to kerogen Di9S1, and are consistent with HI values and H/C atomic ratios of these three samples (Tables 1 and 3 and Figure 6a,g). Therefore, the higher HI value and H/C ratio cannot be fully ascribed to the higher concentrations of volatile aromatic hydrocarbons and phenols for kerogen Di9S1 compared with the two coals. This issue will be further discussed later.

4.2. Generation of Gaseous Hydrocarbons. The maximum yields of ethane, propane, butanes, and pentanes are similar between coal FM1C2 and kerogen Di9S1 at 20 °C/h, but they are relatively higher for coal FM1C2 than kerogen Di9S1 at 2 °C/h. However, the maximum yields of wet gases for these two samples differ strikingly from those of coal J23C1. The maximum yields of ethane, propane, butanes, and pentanes for coal FM1C2 and kerogen Di9S1 are about 4, 10, 20, and and 80 times, respectively, those of coal J23C1 (Table 3 and Figure 6b–e). For gas components generated from these three samples, the amounts of wet gases relative to methane appear closely related to HI, H/C atomic ratio, and relative concentration of aliphatic carbon to aromatic carbon in

DOI: 10.1021/acs.energyfuels.6b01143
Energy Fuels 2017, 31, 73–94

kerogen, and are substantially lower than pyrolyzing products from oil-prone kerogens and oils.[52−54,63]

In the confined pyrolysis experiments, gaseous hydrocarbons were generated from the primary-cracking of solid kerogen and secondary-cracking of oil components which themselves were generated from kerogen thermal degradation.[23,64,65] Previous studies demonstrated that the amounts of total wet gases generated from oil-cracking are in the range 300−400 mg/g oil in confined pyrolysis for oil alone, oil plus minerals, and oil plus pyrobitumen.[53,54] For coal J23C1, the maximum amounts of total liquid *n*-alkanes ($\sum n\text{-}C_{8+}$) and oil are about 2 and 9 times, respectively, of the maximum amount of the total wet gases ($\sum C_{2-5}$) (Table 3, and Figures 5 and 6). It can be determined that wet gases (C_{2-5}) were mainly generated from the secondary-cracking of oil components for this sample.

For coal FM1C2, the maximum amount of total liquid *n*-alkanes ($\sum n\text{-}C_{8+}$) is relatively lower than the maximum amount of the total wet gases ($\sum C_{2-5}$). However, the maximum amounts of total liquid components ($\sum C_{8+}$) and oil are about 3- and 5-fold, respectively, of the maximum amount of total wet gases (Table 3, and Figures 5 and 6). Therefore, it is reasonable to suggest that wet gases were mainly generated from the secondary-cracking of oil components for this sample, just as coal J23C1.

For kerogen Di9S1, the maximum amount of total wet gases is 5−6-fold that of coal J23C1. However, the maximum amounts of total liquid *n*-alkanes ($\sum n\text{-}C_{8+}$) and oil are just similar, or even lower than that of coal J23C1. It can be estimated that, for kerogen Di9S1, wet gases were mainly generated from the primary-cracking of solid kerogen (>80%) with minor contributions from the secondary-cracking of oil components (<20%). The yields of individual wet gases and the total are significantly higher for kerogen Di9S1 than for coal FM1C2 at lower temperatures and EASY%Ro values and opposite at higher temperatures and EASY%Ro values (Figure 6b−f). This result can be also ascribed to the different formation mechanisms and origins of these wet gases between kerogen Di9S1 and coal FM1C2. For keogen Di9S1, wet gases were mainly generated from primary-cracking of kerogen while for coal FM1C2, they were mainly generated from secondary-cracking of oil components. In principle, wet gases formed relatively earlier at lower maturities from primary-cracking of kerogen than secondary-cracking of oil components.[2,23]

For all three samples J23C1, FM1C2, and Di9S1, the yields of liquid components and oil generally increase from EASY%Ro 0.5 to maximum values at EASY%Ro 1.0−1.2, and then decrease rapidly to EASY%Ro 2.0 (Figure 5b−c), demonstrating that the cracking of liquid components mainly occurred at EASY%Ro ranging 1.0−2.0. For coals J23C1 and FM1C2, the yields of individual wet gases and the total ($\sum C_{2-5}$) are generally very low at EASY%Ro < 1.0, and increase rapidly from EASY%Ro 1.0 to maximum values at EASY%Ro 1.8−2.2 (Figure 6b−f), consistent with the major stage of oil cracking (Figure 5b−c). However, for kerogen Di9S1, the yields of individual wet gases and the total ($\sum C_{2-5}$), especially of C_3−C_5, are substantially high at EASY%Ro 1.0, and increase rapidly from EASY%Ro 0.5 to maximum values at EASY%Ro 1.0−1.8 (Figure 6b−f), inconsistent with the results from the major oil-cracking stage (Figure 5b,c). These results also demonstrate that wet gases were mainly generated from secondary-cracking of oil for J23C1 and FM1C2 while they were mainly generated from the primary-cracking of kerogen for Di9S1.

Previous studies demonstrated that methane yield is around 430 mg/g oil in oil pyrolysis experiments at EASY%Ro 4.46.[53,54,63] The measured maximum amounts of oil components are 59.37, 175.75, and 80.75 mg/g TOC, respectively, for J23C2, FM1C2, and Di9S1 (Table 3 and Figure 6c). The amounts of methane from secondary-cracking of the generated oil would be about 25.53, 75.57, and 34.72 mg/g TOC, comprising up to 28.3%, 48.2%, and 17.6% of the total methane yields, respectively, for the three samples at EASY%Ro 4.43 (Table 3 and Figure 6a). Numerous previous studies demonstrated that the primary-cracking of coal and type III kerogen produced mainly methane with minor amounts of wet gases while oil cracking produced mainly wet gases during pyrolysis.[53,54,58,61,66−74] The result of the present study is consistent with these previous studies.

According to methane yield variation with maturity (Figure 6a), methane generation can be divided into the following three stages:

(1) At EASY%Ro < 1.0, methane yield is generally low. Methane was mainly generated from primary-cracking of kerogen for all the three samples.
(2) Within EASY%Ro in the range 1.0−3.5, methane yield increased substantially. Methane was generated both from primary-cracking of kerogen and secondary-cracking of oil and wet gases.
(3) At EASY%Ro > 3.5, methane yield further increased rapidly for J23C1 and Di9S1 but slowly for FM1C2. Methane was mainly generated from primary-cracking of kerogen (residual solid organic matter).

4.3. Kerogen Structures. From ^{13}C NMR spectra, the ratio (R1) for the concentration of aliphatic carbon to aromatic carbon decreases from kerogen Di9S1 (0.639), through coal FM1C2 (0.530) to coal J23C1 (0.145, Table 2 and Figure 3), consistent with HI values and H/C atomic ratios of these three samples (Table 1). However, the ratio (R2) for the concentration of methyl groups, including terminal methyl and methyl on aromatic ring, to methylene groups, including cyclic and acyclic methylene and methylene on aromatic ring, increases from kerogen Di9S1 (0.560), through coal J23C1 (0.717), to coal FM1C2 (1.20, Table 2 and Figure 2).

Kerogen Di9S1 produced a higher amount of gaseous hydrocarbons and a lower amount of oil compared with coal FM1C2 (Figures 5 and 6). This result may suggest that the former contains a higher amount of methyl and short-chain alkane moieties with carbon number <7 and a lower amount of long-chain alkane moieties with carbon number >7 attached to aromatic nuclei compared with the latter. In this case, kerogen Di9S1 should have higher R2 ratio than coal FM1C2, in contrast to the result from ^{13}C NMR spectra analysis (Table 2 and Figure 3).

Kerogen Di9S1 yields higher amounts of toluene and xylenes compared with coal FM1C2 (Table 3, and Figures 4 and 5d). We deduce that kerogen Di9S1 possibly mainly contains crossed alkane moieties with both terminals attached to aromatic rings based on the concentration of methyl group relative to the methylene group (R2) from ^{13}C NMR spectra. The crossed alkane moieties were hardly released as liquid alkanes but possibly further cracked into gaseous components during pyrolysis. In contrast, coal FM1C2 possibly mainly contains alkane moieties with only one terminal attached to the aromatic ring, which can be easily released as liquid alkanes during pyrolysis. Coal J23C1 has a substantially lower HI, H/C

DOI: 10.1021/acs.energyfuels.6b01143
Energy Fuels 2017, 31, 73−94

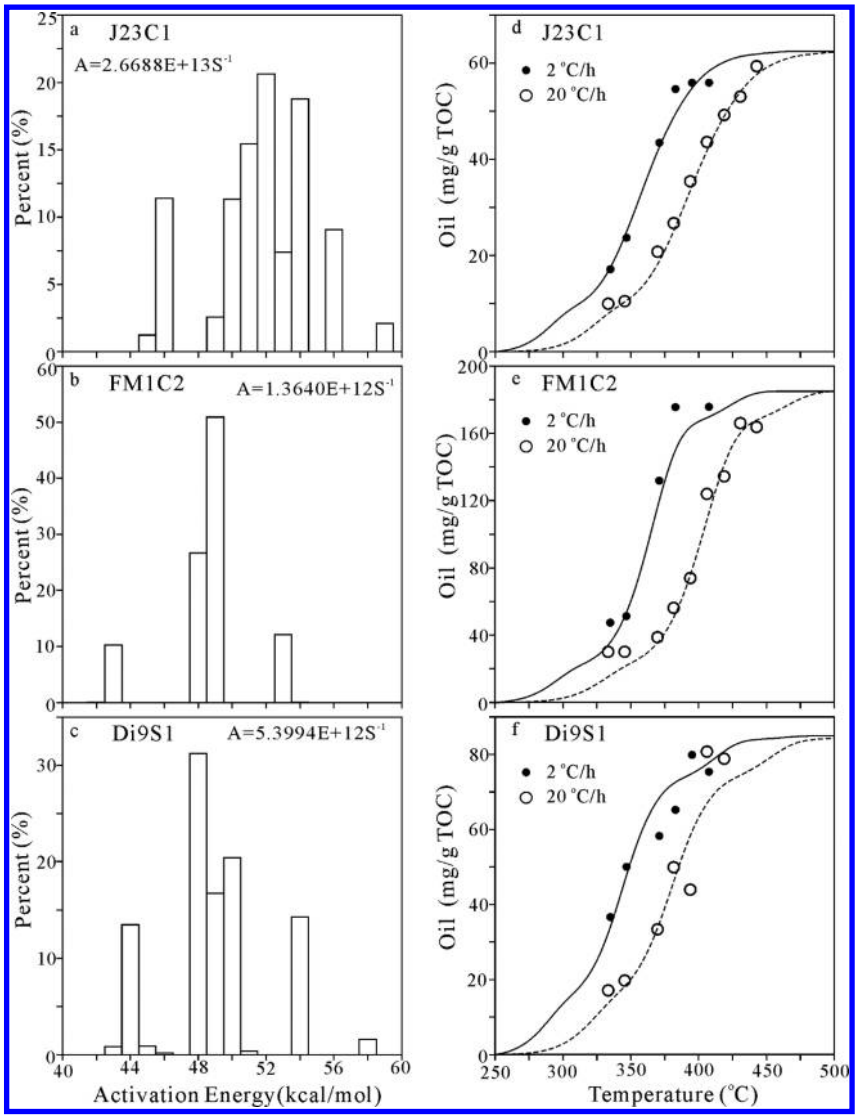

Figure 7. Activation energy distributions and frequency factors for oil generation (left), and the fit of calculated cumulative amounts of oil with measured results (right)

atomic ratio, and ratio of the concentration of aliphatic carbon to aromatic carbon (R1), and yielded a much lower amount of gaseous hydrocarbons than coal FM1C2 and kerogen Di9S1; however, it yielded an amount of liquid components similar to kerogen Di9S1. This result suggests that coal J23C1 mainly contains alkane moieties with only one terminal attached to aromatic ring, just as coal FM1C2 but different from kerogen Di9S1.

Kerogen Di9S1 appears sensitive to heating rates during pyrolysis because it contains mainly crossed alkane moieties. For this kerogen, reaction pathways and mechanisms for oil and gas generations are likely different, leading to the different yields of wet gases and monoaromatic components and ratios of $C_1/\sum C_{1-5}$ and methylnaphthalenes/(methylnaphthalenes + 2 × n-C_{13}) between the two heating rates 2 and 20 °C/h (Figures 5 and 6).

Kerogens for coaly source rocks can be classified into two end groups based on their structures. Group 1 kerogens contain mainly alkane moieties with only one terminal attached to aromatic rings, such as coals J23C1 and FM1C2, while group 2 kerogens contain mainly crossed alkane moieties with both terminals attached to the aromatic ring, such as kerogen Di9S1. If coaly source rocks contain mainly group 1 kerogen, their oil generative potentials are closely related to H/C atomic ratios and HI values. However, if coaly source rocks contain mainly group 2, or/and intermediate type of kerogens between groups 1 and 2, their oil generative potentials may have no relationship to H/C atomic ratios and HI values as demonstrated by kerogen Di9S1. This result is consistent with the previous studies.[19,20]

The differences in chemical compositions of kerogen among J23C1, FM1C2, and Di9S1 can be ascribed to both biological precursors and depositional environments.[1,2] Coal J23C1 was mainly derived from hydrogen-poor terrigenous high plant debris and deposed in relative oxidative environment, and therefore, it contains less aliphatic moieties. In contrast, coal FM1C2 and kerogen Di9S1 were derived from hydrogen-rich terrigenous plant debris, possibly mixed with aquatic algae remains, and deposited in relatively anoxic environments; therefore, they contain more aliphatic moieties. It is unclear to us whether the differences in network structures of kerogen among J23C1, FM1C2, and Di9S1, i.e., terminal alkane moieties in J23C1 and FM1C2 and crossed alkane moieties in Di9S1, were mainly caused by differences in biological

DOI: 10.1021/acs.energyfuels.6b01143
Energy Fuels 2017, 31, 73−94

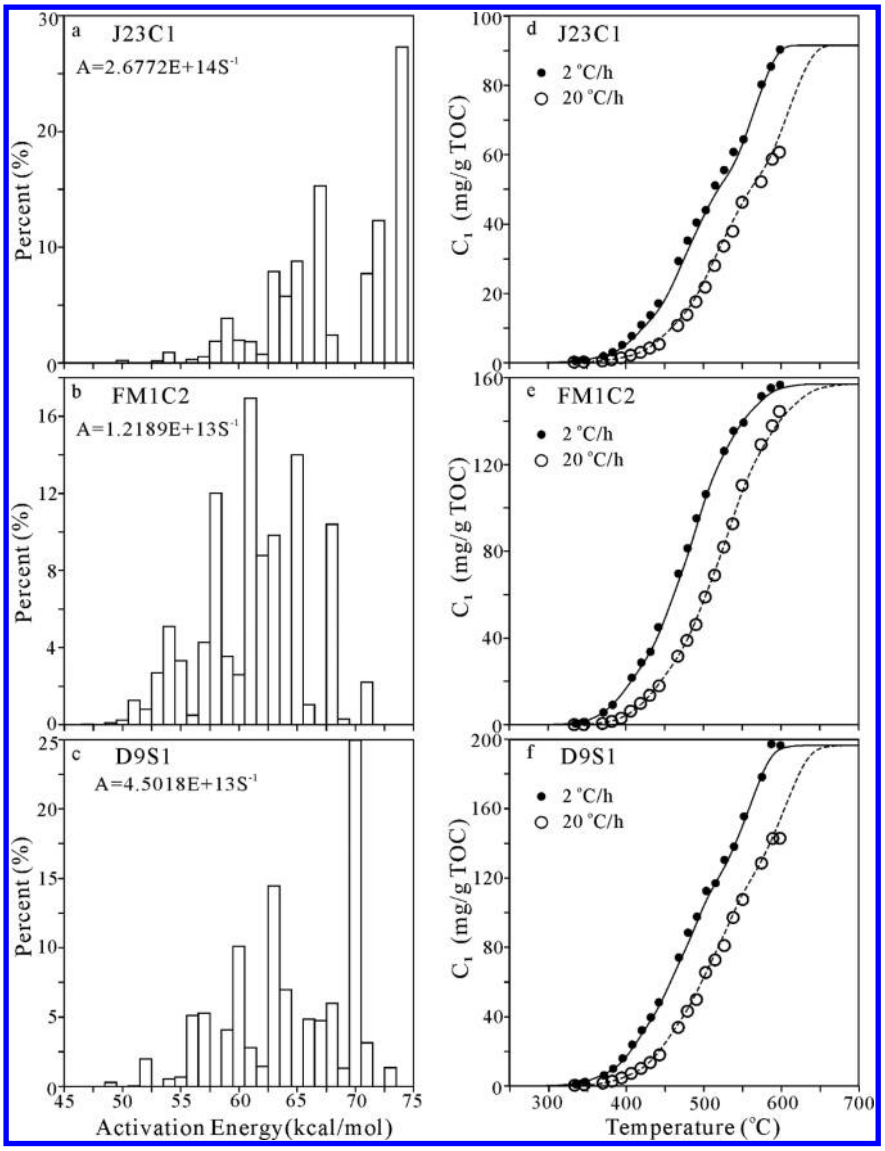

Figure 8. Activation energy distributions and frequency factors for methane generation (left), and the fit of calculated cumulative amounts of methane with measured results (right).

precursors or chemical and bacterial modifications during diagenesis.

4.4. Mineral Catalytic Influence. Coal samples J23C1 and FMC2 were not treated with HCl and HF. However, these two coals have very high TOC, i.e., 68.79% and 71.48%, respectively (Table 1), and contain very low amounts of minerals, including clay minerals. In contrast, kerogen Di9S1 has a lower TOC, i.e., 30.63%, and contains relatively higher amounts of minerals. Previous studies demonstrated that, for organic-rich immature source rocks, whole-rock samples yield kinetic parameters similar to those for kerogen.[75−77] Therefore, mineral catalytic influence on oil and gas generation from the coal and kerogen samples in the present study is insignificant.

4.5. Kinetic Modeling for Hydrocarbon Generation. *4.5.1. Kinetic Parameters for Oil Generation.* Hydrocarbon generation from kerogen is generally described using a set of parallel first-order reactions with a single frequency factor and a distribution of activation energies.[58,66,69,78,79] The measured maximum oil yields are 59.37 and 55.94 mg/g TOC at 20 and 2 °C/h, respectively, for coal J23C1; 166.06 and 175.75 mg/g TOC at 20 and 2 °C/h, respectively, for coal FM1C2; and 80.75 and 79.88 mg/g TOC at 20 and 2 °C/h, respectively, for kerogen Di9S1. We assume that the measured maximum oil yield represents a 95% transformation ratio for the three samples considering the overlap between oil generation and cracking. The maximum oil yields could be 62.50 mg/g TOC (59.37/0.95) for coal J23S3, 185.00 mg/g TOC (175.75/0.95) for coal FM1C2, and 85.00 mg/g TOC (80.75/0.95) for kerogen Di9S1. The maximum oil yields for these three samples are approximate only due to scarce measured data.

Kinetic parameters for oil generation from these three samples were optimized using Kinetics 2000 software and are shown in Figure 7a−c. The fits of the cumulative oil yields calculated from the kinetic parameters and measured from confined pyrolysis experiments are shown in Figure 7d−f. For coal J23C1, activation energy values range from 45 to 59 kcal/mol, and average 51.73 kcal/mol with a frequency factor 2.6688×10^{13} s^{-1}. For coal FM1C2, activation energy values range from 42 to 54 kcal/mol, and average 48.60 kcal/mol with a frequency factor 1.3640×10^{12} s^{-1}. For kerogen Di9S1, activation energy values range from 43 to 58 kcal/mol, and

DOI: 10.1021/acs.energyfuels.6b01143
Energy Fuels 2017, 31, 73−94

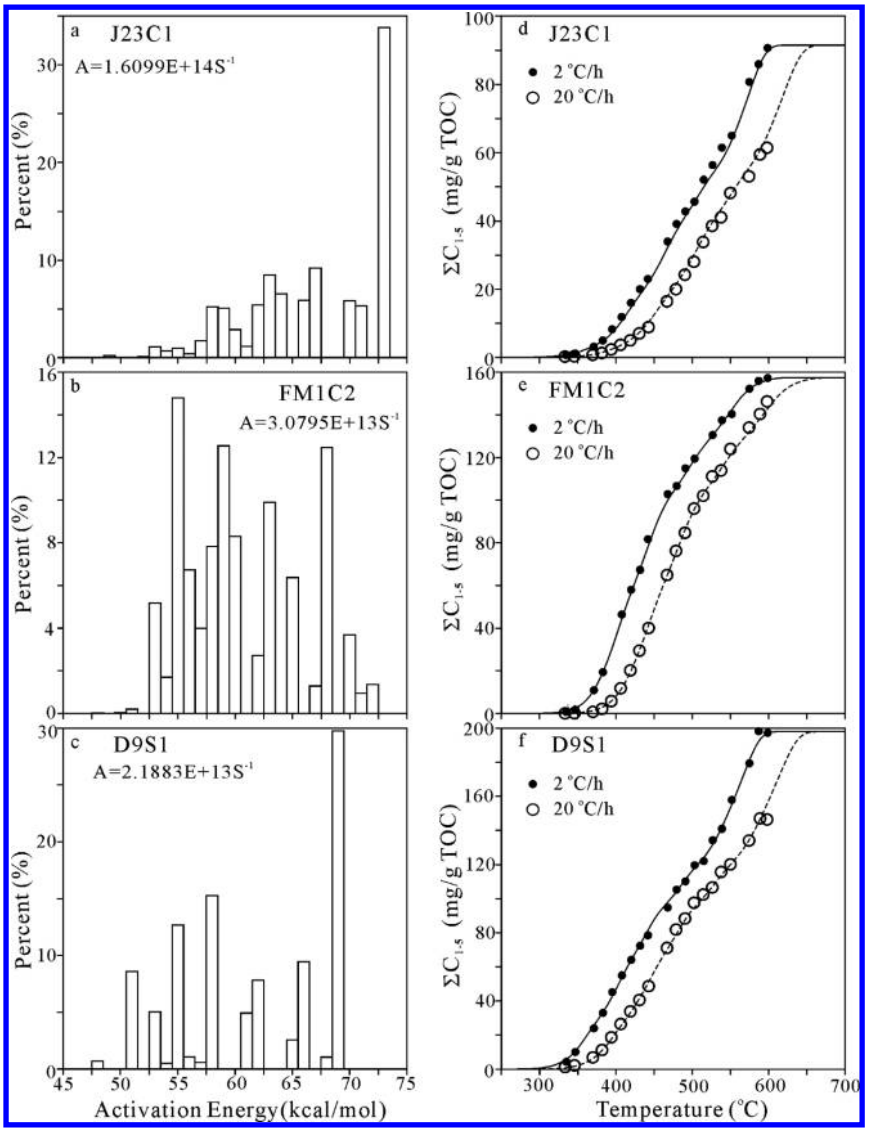

Figure 9. Activation energy distributions and frequency factors for the generation of the total gaseous hydrocarbons (left), and the fit of calculated cumulative amounts of the total gaseous hydrocarbons with measured results (right).

average 48.99 kcal/mol with a frequency factor 5.3994×10^{12} s^{-1}.

4.5.2. Kinetic Parameters for Generation of Methane and Total Gaseous Hydrocarbons ($\sum C_{1-5}$). At heating rate 2 °C/h, from 551.6 to 598.6 °C, the yields of methane and total gaseous hydrocarbons ($\sum C_{1-5}$) for coal J23C1 increase rapidly and consistently from 64.42 to 90.32 and from 64.99 to 90.69 mg/g TOC, respectively. We set both the maximum yields of methane and total gaseous hydrocarbons ($\sum C_{1-5}$) for coal J23C1 as 91.50 mg/g TOC. For coal FM1C2, the yields of methane and total gaseous hydrocarbons ($\sum C_{1-5}$) increase slowly from 139.33 to 156.73 and from 140.38 to 157.24 mg/g TOC, respectively, at this temperature range. We set the maximum yields of methane and total gaseous hydrocarbons ($\sum C_{1-5}$) for coal FM1C2 as 157.00 and 157.50 mg/g TOC, respectively. For kerogen Di9S1, the yields of methane and total gaseous hydrocarbons ($\sum C_{1-5}$) increase rapidly from 155.50 to 197.18 and from 157.93 to 198.15 mg/g TOC, respectively, within 551.6−586.8 °C, but decrease to 196.46 and 197.22 mg/g TOC, respectively, at 598.6 °C. We set the maximum yields of methane and total gaseous hydrocarbons ($\sum C_{1-5}$) for kerogen Di9S1 as 196.50 and 198.00 mg/g TOC, respectively.

Kinetic parameters for the generation of methane and total gaseous hydrocarbons from these two samples were optimized using Kinetics 2000 software and are shown in Figures 8a−c and 9a−c. The fits of the cumulative yields of methane and total gaseous hydrocarbons calculated from the kinetic parameters and measured from confined pyrolysis experiments are shown in Figures 8d−f and 9d−f.

For coal J23C1, the activation energy values average 68.15 and 66.78 kcal/mol with frequency factors 2.6772×10^{14} and 1.6099×10^{14} s^{-1} for the generation of methane and total gaseous hydrocarbons, respectively. For coal FM1C2, the activation energy values average 61.21 and 60.50 kcal/mol with frequency factors 1.2189×10^{13} and 3.0795×10^{13} s^{-1} for the generation of methane and total gaseous hydrocarbons, respectively. For kerogen Di9S1, the activation energy values average 64.34 and 61.42 kcal/mol with frequency factors 4.5018×10^{13} and 2.1883×10^{13} s^{-1} for the generation of methane and total gaseous hydrocarbons, respectively.

DOI: 10.1021/acs.energyfuels.6b01143
Energy Fuels 2017, 31, 73−94

Table 4. Measured Transformation Ratios to the Generations of Methane and Total Gaseous Hydrocarbons ($\sum C_{1\text{-}5}$)

		J23C1		FM1C2		Di9S1	
T (°C)	EASY%R_o	C_1	$\sum C_{1-5}$	C_1	$\sum C_{1-5}$	C_1	$\sum C_{1-5}$
				20 °C/h			
333.3	0.56	0.0023	0.0030	0.0004	0.0005	0.0023	0.0065
345.5	0.61	0.0029	0.0037	0.0007	0.0008	0.0034	0.0113
369.7	0.72	0.0061	0.0085	0.0038	0.0049	0.0088	0.0351
381.6	0.78	0.0097	0.0142	0.0098	0.0139	0.0142	0.0569
393.8	0.85	0.0158	0.0258	0.0191	0.0368	0.0238	0.0944
406.1	0.94	0.0242	0.0406	0.0401	0.0752	0.0369	0.1335
418.8	1.05	0.0329	0.0547	0.0628	0.1283	0.0515	0.1712
430.7	1.18	0.0468	0.0774	0.0865	0.1873	0.0690	0.2050
442.7	1.31	0.0590	0.0973	0.1143	0.2545	0.0912	0.2459
466.8	1.62	0.1179	0.1799	0.2011	0.4121	0.1717	0.3593
478.6	1.79	0.1517	0.2188	0.2475	0.4840	0.2191	0.4135
490.2	1.97	0.1927	0.2650	0.2943	0.5379	0.2531	0.4461
502.1	2.16	0.2385	0.3067	0.3752	0.6098	0.3324	0.4929
514.2	2.37	0.3068	0.3697	0.4392	0.6482	0.3691	0.5171
526.0	2.58	0.3678	0.4217	0.5220	0.7056	0.4112	0.5382
537.6	2.79	0.4145	0.4490	0.5904	0.7234	0.4933	0.5841
549.8	3.02	0.5060	0.5267	0.7034	0.7874	0.5461	0.6067
574.1	3.46	0.5708	0.5800	0.8229	0.8510	0.6525	0.6770
588.6	3.70	0.6415	0.6501	0.8781	0.8915	0.7246	0.7425
597.8	3.84	0.6636	0.6715	0.9203	0.9287	0.7253	0.7396
				2 °C/h			
334.9	0.72	0.0058	0.0078	0.0036	0.0045	0.0052	0.0220
346.8	0.78	0.0090	0.0128	0.0084	0.0116	0.0119	0.0512
371.0	0.95	0.0214	0.0346	0.0363	0.0694	0.0313	0.1212
382.9	1.07	0.0340	0.0546	0.0584	0.1229	0.0508	0.1670
395.1	1.21	0.0563	0.0904			0.0809	0.2281
407.6	1.35	0.0844	0.1297	0.1381	0.2947	0.1209	0.2777
419.8	1.51	0.1196	0.1750	0.1825	0.3683	0.1631	0.3237
431.5	1.68	0.1499	0.2188	0.2143	0.4275	0.2007	0.3657
441.8	1.85	0.1875	0.2515	0.2867	0.5190	0.2449	0.3964
467.6	2.29	0.3206	0.3714	0.4438	0.6530	0.3761	0.4787
479.4	2.51	0.3853	0.4276	0.5183	0.6771	0.4488	0.5317
490.9	2.73	0.4422	0.4677	0.6063	0.7298	0.4955	0.5564
502.9	2.97	0.4808	0.4989	0.6770	0.7582	0.5711	0.6039
514.9	3.21	0.5588	0.5693			0.5938	0.6163
526.5	3.43	0.6074	0.6160	0.8042	0.8287	0.6620	0.6780
538.7	3.65	0.6644	0.6720	0.8630	0.8725	0.7008	0.7119
551.6	3.86	0.7040	0.7103	0.8874	0.8913	0.7893	0.7976
574.7	4.17	0.8768	0.8824	0.9651	0.9665	0.9046	0.9060
586.8	4.31	0.9338	0.9391	0.9893	0.9899	1.0009	1.0008
598.6	4.43	0.9871	0.9912	0.9983	0.9983	0.9973	0.9960

Measured transformation ratios to the generations of methane and the total gaseous hydrocarbons ($\sum C_{1-5}$) for the three samples are demonstrated in Table 4 and Figure 10. At oil window with EASY%Ro 0.56−1.35%, transformation ratios to methane generations range 0.0023−0.0841, 0.0004−0.1381, and 0.0023−0.1209 for samples J23C1, FM1C2, and Di9S1, respectively. Transformation ratios to the generation of the total gaseous hydrocarbons range 0.0030−0.1297, 0.0005−0.2947, and 0.0065−0.2777 for the three samples, respectively.

At wet gas window with EASY%Ro 1.51−2.16%, transformation ratios to methane generations range 0.1179−0.2385, 0.1825−0.4438, and 0.1631−0.3761 for samples J23C1, FM1C2, and Di9S1, respectively. Transformation ratios to the generation of the total gaseous hydrocarbons range 0.1750−0.3067, 0.3683−0.6530, and 0.3237−0.4787 for the three samples, respectively.

At dry gas window with EASY%Ro 2.29−4.43%, transformation ratios to methane generations range 0.3068−0.9871, 0.4392−0.9983, and 0.3691−0.9973 for samples J23C1, FM1C2, and Di9S1, respectively. Transformation ratios to the generation of the total gaseous hydrocarbons range 0.3697−0.9912, 0.6482−0.9983, and 0.4787−0.9980 for the three samples, respectively. For coal J23C1, about 69.3% methane and 63.0% total gaseous hydrocarbons were generated at a dry gas window. For coal FM1C2, about 56.1% methane and 35.2% total gaseous hydrocarbons were generated at a dry gas window. For kerogen Di9S1, about 63.1% methane and 52.1% total gaseous hydrocarbons were generated at a dry gas window.

A jump of methane generation can be observed for coal J23C1 within EASY%Ro 3.86−4.43% and for kerogen Di9S1 within EASY%Ro 3.65−4.31%. However, this jump cannot be

DOI: 10.1021/acs.energyfuels.6b01143
Energy Fuels 2017, 31, 73−94

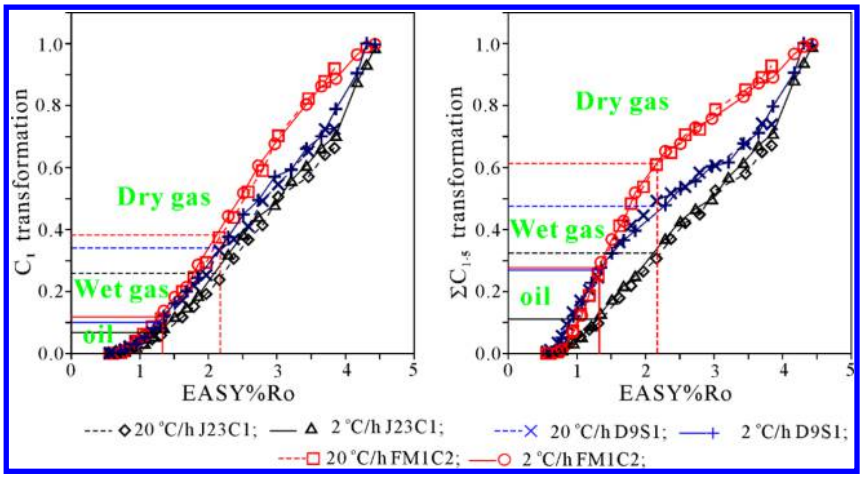

Figure 10. Measured transformation ratios to the generations of methane and the total gaseous hydrocarbons ($\sum C_{1-5}$) versus vitrinite reflectance (EASY%Ro)

Table 5. Generation of Oil and Gaseous Hydrocarbons for J23C1, FM1C2, and Di9S1 at 5 °C/my[a]

	J23C1		FM1C2		Di9S1	
TR	*T* (°C)	EASY%Ro (%)	*T* (°C)	EASY%Ro (%)	*T* (°C)	EASY%Ro (%)
			Oil Generation			
0.10	101.4	0.54	99.9	0.53	93.6	0.49
0.30	132.5	0.76	130.5	0.75	120.5	0.67
0.50	143.2	0.86	137.4	0.79	128.5	0.73
0.70	154.2	0.99	143.2	0.86	137.8	0.80
0.90	171.0	1.28	164.0	1.16	169.5	1.25
			Gas Generation			
0.10	187.6	1.61	173.1	1.32	160.8	1.11
0.30	225.3	2.60	191.8	1.71	194.9	1.78
0.50	255.8	3.51	215.2	2.31	234.0	2.86
0.70	294.0	4.34	244.9	3.20	282.5	4.13
0.90	>300	>4.44	288.4	4.24	299.3	4.43

[a]TR: transformation ratio

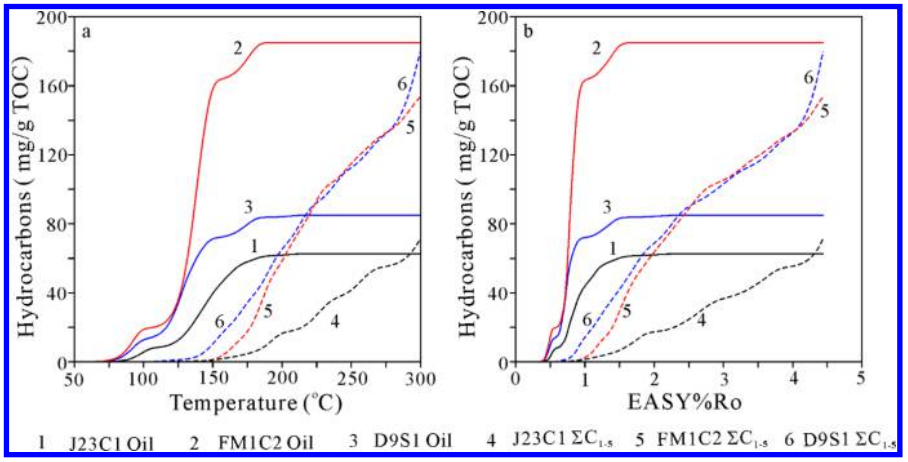

Figure 11. Predicted cumulative amounts of oil and total gaseous hydrocarbons ($\sum C_{1-5}$) generated in closed systems under geological conditions at 5 °C/my for J23C1 and FM1C2 and Di9S1 versus temperature (left) and EASY%Ro (right).

observed for coal FM1C2 (Figure 6a,g). Within this maturity range, the amounts of wet gases are minor compared with the increasing methane yields (Figure 6f), and therefore, methane was mainly generated from solid organic matter. A spectacular high portion for a high activation energy value can be observed accordingly from the distribution of activation energies for the generation of methane and total gaseous hydrocarbons for coal J23C1 and kerogen Di9S1, but not for coal FM1C2 (Figures 8 and 9). Peters et al.[77,80] demonstrated that oil-prone source rocks, having similar organic matter based on Rock-Eval pyrolysis or petrographic analysis, can display a broad range of kinetic response for kerogen decomposition to petroleum. Coal and gas-prone kerogen have greater heterogeneity in composition and structure than oil-prone kerogen.[2,81] The

DOI: 10.1021/acs.energyfuels.6b01143
Energy Fuels 2017, 31, 73−94

substantial differences in kinetic properties among the three samples are consistent with the previous studies.[77,80]

4.6. Hydrocarbon Generation in Central and Southern Junggar Basin. Under geological conditions at 5 °C/My, temperatures and EASY%Ro values for 10−90% transformation to oil generation are 101.4−171.0, 99.9−164.0, and 93.6−169.5 °C, and 0.54−1.28%, 0.53−1.16%, and 0.49−1.25% for J23C1, FM1C2, and Di9S1, respectively (Table 5 and Figure 11). Temperatures and EASY%Ro values for 10−50% transformation to the generation of total gaseous hydrocarbons ($\sum C_{1-5}$) are 187.6−255.8 °C, 173.1−215.2, and 160.8−234.0 °C, and 1.61−3.51%, 1.32−2.31%, and 1.11−2.86%, respectively, for J23C1, FM1C2, and Di9S1 (Table 5 and Figure 11).

In Junggar Basin, the depth and maturity of Jurassic source rocks generally increase from the north to the south (Figure 1).[27,47,49−51] Jurassic source rocks are in the oil generative window with EASY%Ro ranging from 0.6% to 1.4% in a large area in the central and southern Junggar Basin while they are in condensate-wet gas and dry gas windows with EASY%Ro > 1.4 in a limited area in the southern Junggar Basin (Figure 1). At the three locations S, F, and W, the Jurassic source rocks are in oil, condensate-wet gas, and dry gas generative windows, respectively (Figure 1). The burial histories for the Jurassic strata at these three locations are demonstrated in Figure 12 on the basis of seismic data. At location W, the Jurassic source rocks have the deepest burial and highest maturity in the basin. The initial oil and gas generative potentials (maximum oil and gas yields) and kinetic parameters for gas and oil generation for the Jurassic coaly source rocks may vary substantially in the Junggar Basin. Here, we tentatively modeled oil and gas generation from the Lower Jurassic Badaowan Formation (J_{1b}) using kinetic parameters for samples FM1C2 and Di9S1, and from the Middle Jurassic Xishanyao Formation (J_{2x}) using kinetic parameters for sample J23C1 at the three locations. The maturation histories and hydrocarbon generation for the source rocks within the Badaowan and Xishanyao formations at the three locations are demonstrated in Figures 13−15, respectively. The accumulative yields of oil and the total gaseous hydrocarbons ($\sum C_{1-5}$) generated from the source rocks within the two formations at present are shown in Table 6.

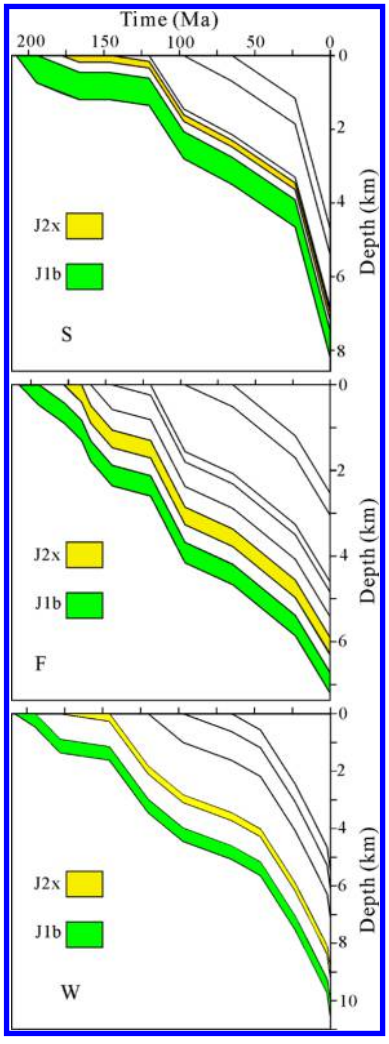

Figure 12. Burial histories for Jurassic strata at locations S, F, and W in the southern Junggar Basin.

For Jurassic source rocks at these three locations, the accumulative oil yields are mainly controlled by initial oil generative potentials (the maximum oil yields). Transformation ratios for oil generation calculated from the kinetic parameters for the three samples range 0.803−1.00. The accumulative gas yields ($\sum C_{1-5}$) are controlled by both the initial gas generative potentials (the maximum gas yields) and transformation ratios. Sample J23C1 has the lowest initial gas generative potential (maximum gas yield) and the lowest transformation ratio at the same thermal stress level among the three samples. The accumulative gas yield for J23C1 is very low even at location W (Table 6 and Figure 15d).

Previous studies demonstrated that (1) residual oil in source rock in natural systems is dominantly absorbed by solid kerogen, and (2) the effect of mineral matrix is insignificant to the amount of residual oil.[82−84] These studies suggested that the amount of residual oil is about 100 mg/g CK (organic carbon in kerogen),[83] or ranges 60−90 mg/g of dispersed kerogen after oil expulsion in source rocks.[84] In addition, Sandvik et al.[84] suggested that absorption levels of residual oil in coals may be lower than levels in dispersed kerogen. In the present study, we assume that the amount of residual oil is 100 mg/g TOC in Jurassic coaly source rocks of Junggar Basin after oil expulsion, referenced from the studies by Sandvik et al.[84] and Pepper and Corvi.[83] At the three locations S, F, and W, the accumulative amounts of expelled oil from coal FM1C2 range 65−85 mg/g TOC (Figures 13−15a). However, no oil can be expelled from coal J23C1 and source rocks Di9S1 because the maximum accumulative amounts of oil generated from these two samples are lower than 100 mg/g TOC (Figures 13−15). So far, several oil fields have been found in the Junggar Basin, including Cainan, Qigu, Duoshanzi, Kayindike, Chunfeng, and Chunguang oil fields (Figure 1), in which oil components were mainly derived from Jurassic coaly source rocks.[24−27]

Pepper and Corvi[83] suggested that the amount of residual gas is about 20 mg/g TOC after oil and gas expulsion in source rocks. If this value is used, no gaseous hydrocarbons can be expelled as the gas phase out of the three source rock samples at location S (Figure 13). However, gas components can be dissolved in oil and expelled out of coal FM1C2 as the oil phase. The accumulative amounts of expelled gaseous hydrocarbons would be 8.5 and 21.5 mg/g TOC at location F and 87.6 and 88.7 mg/g TOC at location W for source rocks FM1C2 and Di9S1, respectively (Figures 14 and 15a). For coal J23C1, no gaseous hydrocarbons would be expelled out at both locations F and W (Figures 14 and 15d).

DOI: 10.1021/acs.energyfuels.6b01143
Energy Fuels 2017, 31, 73−94

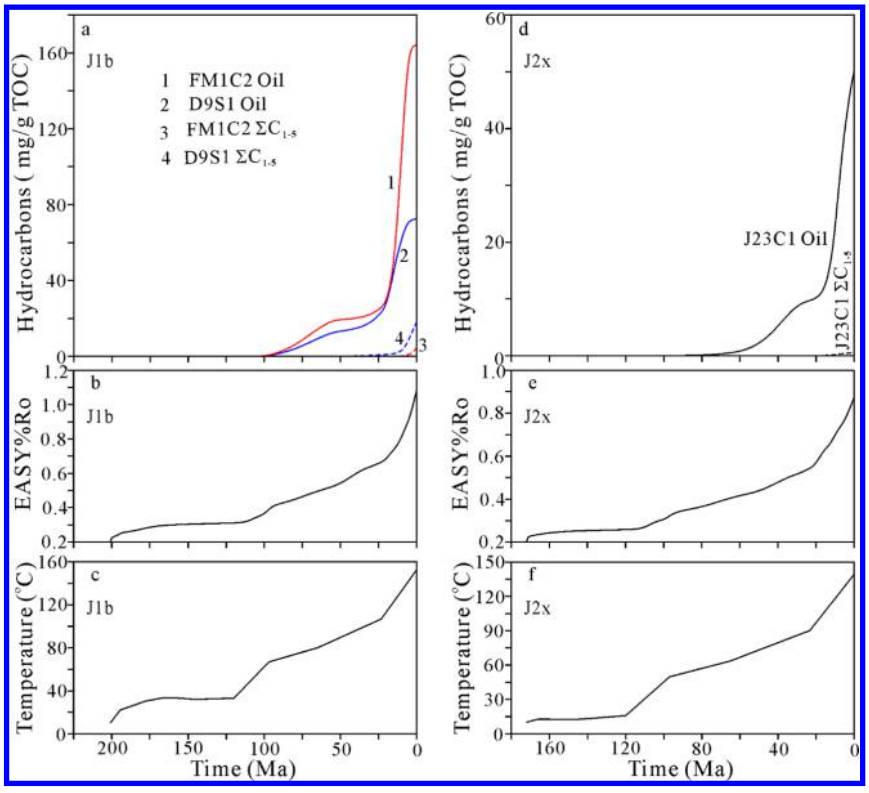

Figure 13. Thermal and hydrocarbon generation histories of source rocks in the middle beds of the Badaowan (left) and Xishanyao formations (right) at location S.

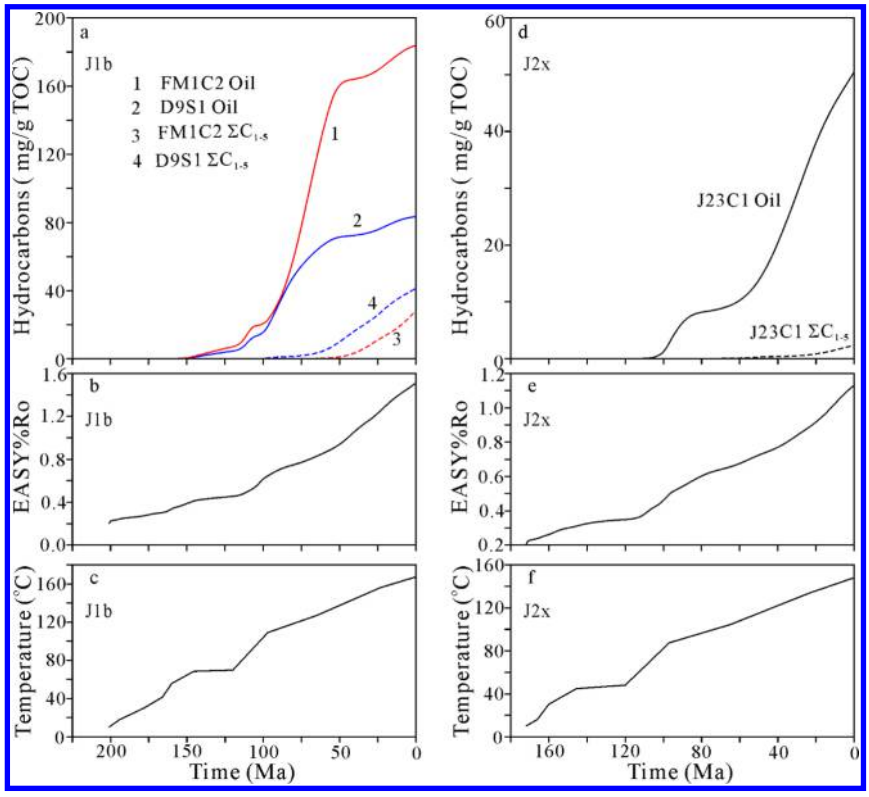

Figure 14. Thermal and hydrocarbon generation histories of source rocks in the middle beds of the Badaowan (left) and Xishanyao formations (right) at location F

In the present study, the maximum accumulative amounts of gaseous hydrocarbons generated from the three source rocks were obtained from a closed confined system. In a natural system, the maximum accumulative amounts of gaseous hydrocarbons generated from source rocks can be reduced due to oil expulsion. For coal FM1C2, the maximum

DOI: 10.1021/acs.energyfuels.6b01143
Energy Fuels 2017, 31, 73−94

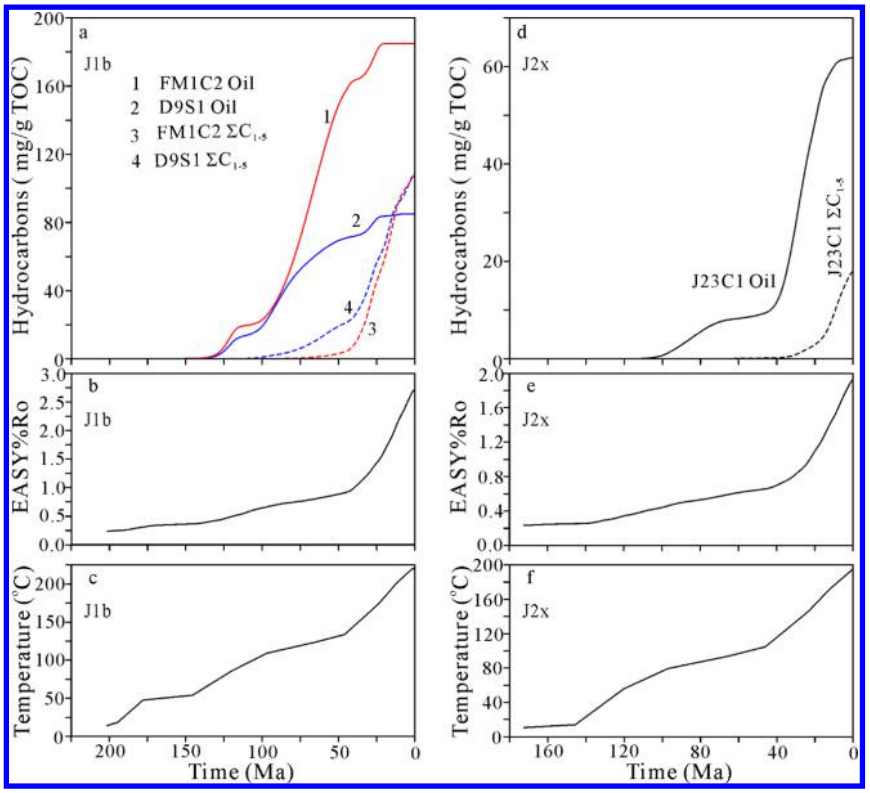

Figure 15. Thermal and hydrocarbon generation histories of source rocks in the middle beds of the Badaowan (left) and Xishanyao formations (right) at location W.

Table 6. Accumulative Yields of Oil and Total Gaseous Hydrocarbons ($\sum C_{1-5}$) Generated from Source Rocks of Badaowan Formation (J_{1b}) and Xishanyao Formation (J_{2x}) at Present in Southern Junggar Basin[a]

	location S		location F		location W	
	oil	$\sum C_{1-5}$	oil	$\sum C_{1-5}$	oil	$\sum C_{1-5}$
J_{1b} (FM1C2)	164.5	4.58	183.9	28.47	185.0	107.64
J_{1b} (Di9S1)	72.7	18.13	83.4	41.50	85.0	108.72
J_{2x} (J23C1)	50.2	0.67	50.5	2.38	61.9	17.98

[a]All data in mg/g TOC.

accumulative expelled oil is about 85 mg/g TOC, assuming that the amount of residual oil is 100 mg/g TOC. The maximum amount of gaseous hydrocarbons generated from oil cracking is about 430 mg/g oil.[53,54,63] In a natural system, the maximum accumulative amount of gaseous hydrocarbons generated from coal FM1C2 would be (157.50−85 × 0.43) = 120.95 mg/g TOC after oil expulsion. The accumulative amounts of gaseous hydrocarbons generated and expelled from the samples at the three locations (S, F, and W) can be significantly lower in a natural system than those predicted in a closed system as demonstrated in Figures 13−15. For coal J23C1 and source rock Di9S1, hydrocarbon generation occurred under closed conditions in nature due to no oil expulsion.

Two gas fields, i.e., Mahe and Hutubi gas fields, have been found in the southern Jungaar Basin after exploration for more than 60 years, in which gaseous hydrocarbons were mainly derived from Jurassic coaly source rocks.[28−30] In the Kuqa depression of Tarim Basin, which is located in the south of the Junggar Basin, a number of giant- and medium-sized gas fields have been found (Figure 16), in which gaseous hydrocarbons were mainly derived from coaly source rocks within Upper Triassic Taliqike Formation (T_{3t}), Lower Jurassic Yangxia Formation (J_{1y}), and Middle Jurassic Kezilenuer Formation (J_{2k}).[34] The amounts of gaseous hydrocarbons found in the

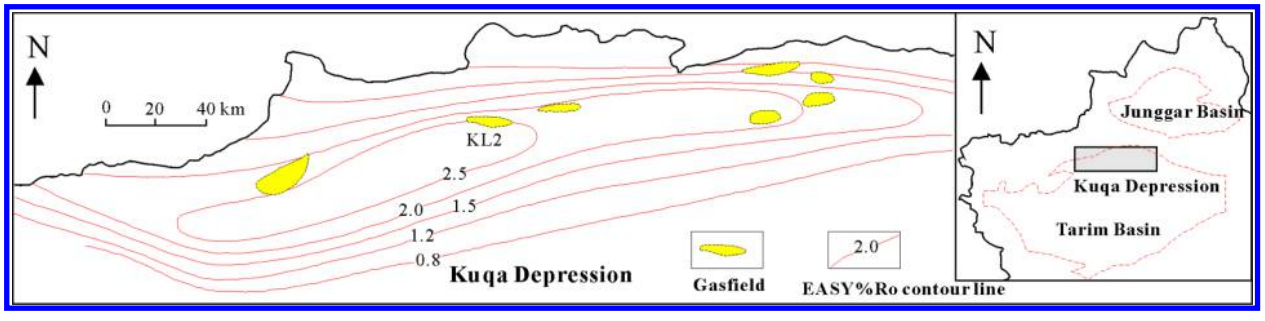

Figure 16. Vitrinite reflectance contour maps (%Ro) at the bottom of the Jurassic strata of the Kuqa (Kuche) Depression in the Tarim Basin (modified after Zhao et al. 2005[34]).

DOI: 10.1021/acs.energyfuels.6b01143
Energy Fuels 2017, 31, 73−94

southern Junggar Basin are negligible compared with those found in the Kuqa depression derived from coaly source rocks. The former is less than 5% of the latter.[35,85] The major factors for the striking difference in the result for coal gas exploration between southern Junggar Basin and Kuqa depression remain unclear. In our opinion, maturity could be an important factor controlling gas generation from coaly source rocks. According to the result of the present study, coaly source rocks do not generate enough gas to start gas phase expulsion in an oil generative window (EASY%Ro 0.6−1.35%, Figures 10, 11, and 13). Only a limited amount of gaseous hydrocarbons can be generated and expelled as the gas phase from coaly source rocks in a condensate-wet gas generative window (EASY%Ro 1.35−2.20%, Figures 10, 11, and 14). A large amount of gaseous hydrocarbons occupying a major part of the initial gas generative potential (maximum accumulative gas yield) is generated from coaly source rocks in dry gas generative window (EASY%Ro > 2.2%, Figures 10−11, 15). Maturities are substantially lower for the Lower and Middle Jurassic source rocks in southern Junggar Basin than the Upper Triassic and Lower−Middle Jurassic coaly source rocks in Kuqa depression (Figures 1 and 16). The dryness ratios ($C_1/\sum C_{1-5}$) range 0.90−0.92 and 0.93−0.95, respectively, for the Mahe and Hutubi gas fields in the southern Junggar Basin.[28−30] For the Kela 2 gas field, the largest in the Tarim Basin, dryness ratios range 0.99−1.00,[34,86,87] much higher than those in southern Junggar Basin, demonstrating that the maturities of source rocks for Kela 2 gas field are extremely high. Kinetic properties for the generation of gaseous hydrocarbons may be also an important controlling factor for effective coaly source rocks. Coal J23C1 is an ineffective source rock within the Middle Jurassic Xishangyao Formation (J_{2x}) at any location of the southern Junggar Basin due to low maximum accumulative gas yield (91.50 mg/g TOC) combined with a lower transformation ratio at the same thermal stress level than the other two samples (Figures 10−15).

In a paper titled "Where Did All the Coal Gas Go?", Patience[88] noted that reservoired gases in mid-Norway were generated predominantly from the marine source rocks, despite the presence of abundant mature coal and terrestrial carboniferous shales in the Lower Jurassic Åre Formation, and suggested that the loss of gas due to poor expulsion and/or complex migration routes in the Åre Formation results in most of the gas not reaching the reservoir. In our opinion, lower transformation ratios for gas generation from coaly source rocks at maturity Ro < 1.4% could also be a critical influencing factor based on the present and previous studies.[22,23,55]

5. CONCLUSIONS

The maximum accumulative oil yields are inconsistent with the maximum accumulative gas yields ($\sum C_{1-5}$) being positively correlated to Rock-Eval hydrogen indices and H/C atomic ratios of kerogen for three coaly source rocks J23C1, FM1C2, and Di9S1. This result is interpreted by the kerogen Di9S1 containing mainly crossed alkane moieties with both terminals attached to aromatic rings while coals J23C1 and FM1C2 contain mainly alkane moieties with only one terminal attached to the aromatic ring based on kerogen ^{13}C NMR spectra, the oil yield relative to gas yield, and the compositions of liquid components produced in confined pyrolysis. The crossed alkane moieties hardly release as liquid alkanes but likely further crack into gaseous components during confined pyrolysis.

Some coaly source rocks within the Jurassic strata are capable of generating enough oil for oil expulsion as demonstrated by the oil yield of coal FM1C2. The amounts of gaseous hydrocarbons generated from the Jurassic coaly source rocks are insignificant in the oil generative window (Ro 0.6−1.35%) due to the low transformation ratio. Elevated maturity (Ro > 1.35%) is a critical controlling factor for the Jurassic coaly source rocks generating sufficient gaseous hydrocarbons and forming commercial gas reservoirs.

■ ASSOCIATED CONTENT

Supporting Information

The Supporting Information is available free of charge on the ACS Publications website at DOI: 10.1021/acs.energyfuels.6b01143.

Kinetic parameters and gas chromatograms (PDF)

■ AUTHOR INFORMATION

Corresponding Author

*Phone: +86 20 85290183. Fax: +86 20 85290706. E-mail: cpan@gig.ac.cn.

Notes

The authors declare no competing financial interest.

■ ACKNOWLEDGMENTS

This study was jointly funded by the National Natural Science Foundation of China (Grant 41572107), the National S&T Major Project of China (Grant 2011ZX05008-002-50), and a grant from Xinjiang Oilfield Company, PetroChina. We thank Prof. Pingan Peng of Guangzhou Institute of Geochemistry, CAS, and Drs. Xulong Wang, Baoli Xiang, Haibo Yang, Jiande Liao, Jiangling Ren, Xiuwei Gao, Ming Wang, and Yi Wang of Xinjiang Oilfield Company, PetroChina, for their kind help and support for this study. We are very grateful to two anonymous reviewers for their constructive reviews and to Dr. Patrick Hatcher for his editorial work. This is contribution No. IS-2320 from GIGCAS.

■ REFERENCES

(1) Hunt, J. M. *Petroleum Geochemistry and Geology*; W. H. Freeman, San Francisco, CA, 1979; p 617.
(2) Tissot, B. P.; Welte, D. H. *Petroleum Formation and Occurrence*; Springer-Verlag: Berlin, 1984; p 699.
(3) Hunt, J. M. Generation of gas and oil from coal and other terrestrial organic matter. *Org. Geochem.* **1991**, *17*, 673−680.
(4) Boreham, C. J.; Powell, T. G. *Org. Geochem.* **1991**, *17*, 723−733.
(5) Clayton, J. L.; Rice, D. D.; Michael, G. E. *Org. Geochem.* **1991**, *17*, 735−742.
(6) Curiale, J. A.; Lin, R. *Org. Geochem.* **1991**, *17*, 785−803.
(7) Fowler, M. G.; Goodarzi, F.; Gentzis, T.; Brooks, P. W. *Org. Geochem.* **1991**, *17*, 681−694.
(8) Fowler, M. G.; Gentzis, T.; Goodarzi, F.; Foscolos, A. *Org. Geochem.* **1991**, *17*, 805−826.
(9) Hagemann, H. W.; Pickel, W. *Org. Geochem.* **1991**, *17*, 839−847.
(10) Difan, H.; Dajiang, Z.; Jinchao, L.; Xiaoming, H. *Org. Geochem.* **1991**, *17*, 827−837.
(11) Katz, B. J.; Kelley, P. A.; Royle, R. A.; Jorjorian, T. *Org. Geochem.* **1991**, *17*, 711−722.
(12) Khorasani, G. K.; Michelsen, J. K. *Org. Geochem.* **1991**, *17*, 849−863.
(13) Landais, P. *Org. Geochem.* **1991**, *17*, 705−710.
(14) Mukhopadhyay, P. K.; Hatcher, P. G.; Calder, J. H. *Org. Geochem.* **1991**, *17*, 765−783.
(15) Pickel, W.; Götz, G. K. E. *Org. Geochem.* **1991**, *17*, 695−704.

DOI: 10.1021/acs.energyfuels.6b01143
Energy Fuels 2017, 31, 73−94

(16) Snowdon, L. R. *Org. Geochem.* **1991**, *17*, 743−747.
(17) Teerman, S. C.; Hwang, R. J. *Org. Geochem.* **1991**, *17*, 749−764.
(18) Peters, K. E. *Am. Assoc. Pet. Geol. Bull.* **1986**, *70*, 318−329.
(19) Isaksen, G. H.; Curry, D. J.; Yeakel, J. D.; Jenssen, A. I. *Org. Geochem.* **1998**, *29*, 23−44.
(20) Killops, S. D.; Funnell, R. H.; Suggate, R. P.; Sykes, R.; Peters, K. E.; Walters, C.; Woolhouse, A. D.; Weston, R. J.; Boudou, J. P. *Org. Geochem.* **1998**, *29*, 1−21.
(21) Sykes, R.; Snowdon, L. R. *Org. Geochem.* **2002**, *33*, 1441−1455.
(22) Dieckmann, V.; Ondrak, R.; Cramer, B.; Horsfield, B. *Mar. Pet. Geol.* **2006**, *23*, 183−199.
(23) Erdmann, M.; Horsfield, B. *Geochim. Cosmochim. Acta* **2006**, *70*, 3943−3956.
(24) Chen, J.; Liang, D.; Wang, X.; Zhong, N.; Song, F.; Deng, C.; Shi, X.; Jin, T.; Xiang, S. *Org. Geochem.* **2003**, *34*, 889−909.
(25) Chen, J.; Deng, C.; Liang, D.; Wang, X.; Zhong, N.; Song, F.; Shi, X.; Jin, T.; Xiang, S. *Org. Geochem.* **2003**, *34*, 911−930.
(26) Chen, J.; Wang, X.; Deng, C.; Zhao, Z.; Ni, Y.; Sun, Y.; Yang, H.; Wang, H.; Liang, D. *Acta Petrolei Sinica* **2015**, *36*, 1315−1331 in Chinese.
(27) Xiao, F.; Liu, L.; Zhang, Z.; Wu, K.; Xu, Z.; Zhou, C. *Org. Geochem.* **2014**, *76*, 48−61.
(28) Chen, S.; Li, Y.; Wang, X.; Abulimiti; Wang, L. *Natural Gas Industry* **2004**, *24* (3), 16−18 in Chinese.
(29) Liao, J.; Zhao, Z.; Ma, W.; Guo, Y.; Shen, N.; Zhou, N. *Xinjiang Geology* **2011**, *29*, 453−456 in Chinese.
(30) Sun, P.; Bian, B.; Yuan, Y.; Zhang, X.; Cao, J. *Geochimica* **2015**, *44*, 275−288 in Chinese.
(31) Dai, J.; Li, J.; Luo, X.; Zhang, W.; Hu, G.; Ma, C.; Guo, J.; Ge, S. *Org. Geochem.* **2005**, *36*, 1617−1635.
(32) Dai, J.; Zou, C.; Qin, S.; Tao, S.; Ding, W.; Liu, Q.; Hu, A. *Mar. Pet. Geol.* **2008**, *25*, 320−334.
(33) Song, Y.; Zhao, M.; Li, B.; Fang, S. *Engineering Sciences* **2010**, *12* (5), 39−45 in Chinese.
(34) Zhao, W.; Zhang, S.; Wang, F.; Cramer, B.; Chen, J.; Sun, Y.; Zhang, B.; Zhao, M. *Org. Geochem.* **2005**, *36*, 1583−1601.
(35) Wang, Y.; Luo, J.; Gao, Q.; Xiang, Y.; Lei, L. *Xinjiang Petroleum Geology* **2012**, *33*, 614−616 in Chinese.
(36) Monthioux, M.; Landais, P.; Monin, J. C. *Org. Geochem.* **1985**, *8*, 275−292.
(37) Monthioux, M.; Landais, P.; Durand, B. *Org. Geochem.* **1986**, *10*, 299−311.
(38) Ohtsuka, Y.; Nozawa, T.; Tomita, A.; Tamai, Y.; Hatano, M. *Fuel* **1984**, *63*, 1363−1366.
(39) Trewhella, M. J.; Poplett, I. J.; Grint, A. *Fuel* **1986**, *65*, 541−546.
(40) Yoshida, T.; Maekawa, Y. *Fuel Process. Technol.* **1987**, *15*, 385−395.
(41) Kuangzong, Q.; Deyu, C.; Zhanguang, L. *Org. Geochem.* **1991**, *17*, 865−872.
(42) Lille, Ü.; Heinmaa, I.; Pehk, T. *Fuel* **2003**, *82*, 799−804.
(43) Almendros, G.; González-Vila, F-J.; Lankes, U.; Knicker, H. *Org. Geochem.* **2008**, *39*, 972−976.
(44) Mao, J.; Chen, N.; Cao, X. *Org. Geochem.* **2011**, *42*, 891−902.
(45) Helms, J. R.; Kong, X.; Salmon, E.; Hatcher, P. G.; Schmidt-Rohr, K.; Mao, J. *Org. Geochem.* **2012**, *44*, 21−36.
(46) Hatcher, P. G.; Ravin, A.; Behar, F.; Baudin, F. *Org. Geochem.* **2014**, *75*, 8−23.
(47) Zhang, G.; Wang, Z.; Wu, M.; Wu, Q.; Yang, B.; Yang, W.; Yang, R.; Fan, G.; Zheng, D.; Zhao, B.; Peng, X.; Yong, T. *Petroleum Geology of Junggar Basin*; Chinese Petroleum Industrial Press, Beijing, 1993; p 390 (in Chinese).
(48) Sweeney, J. J.; Burnham, A. K. *Am. Assoc. Pet. Geol. Bull.* **1990**, *74*, 1559−1570.
(49) Pan, C.; Zhou, Z.; Fan, S.; Xie, Q.; Wang, X.; Wang, Y. *Geochimica* **1997**, *26* (6), 1−7 in Chinese.
(50) Qiu, N.; Zha, M.; Wang, X. *Xinjiang Petroleum Geology* **2000**, *21* (1), 38−41 in Chinese.
(51) Li, P.; Feng, J.; Lu, Y.; Hao, F., Qi, J.; Jiao, Y.; Zhang, Z.; Chen, H. *Tectonic, Sedimentation and Petroleum Formation in Junggar Basin*; Geological Publishing House: Beijing, 2010; p 340 (in Chinese).
(52) Pan, C.; Geng, A.; Zhong, N.; Liu, J.; Yu, L. *Energy Fuels* **2008**, *22*, 416−427.
(53) Pan, C.; Jiang, L.; Liu, J.; Zhang, S.; Zhu, G. *Org. Geochem.* **2010**, *41*, 611−626.
(54) Pan, C.; Jiang, L.; Liu, J.; Zhang, S.; Zhu, G. *Org. Geochem.* **2012**, *45*, 29−47.
(55) Li, E.; Pan, C.; Yu, S.; Jin, X.; Liu, J. *Org. Geochem.* **2013**, *64*, 58−75.
(56) Pan, C.; Yu, L.; Liu, J.; Fu, J. *Earth Planet. Sci. Lett.* **2006**, *246*, 70−89.
(57) Braun, R. L.; Burnham, A. K. *Kinetics GUI.exe, Version 1.11*; 1998.
(58) Behar, F.; Vandenbroucke, M.; Tang, Y.; Marquis, F.; Espitalié, J. *Org. Geochem.* **1997**, *26*, 321−339.
(59) Pepper, A. S.; Corvi, P. J. *Mar. Pet. Geol.* **1995**, *12*, 291−319.
(60) Dieckmann, V. *Mar. Pet. Geol.* **2005**, *22*, 375−390.
(61) Hill, R. J.; Tang, Y.; Kaplan, I. R. *Org. Geochem.* **2003**, *34*, 1651−1672.
(62) Larter, S. R.; Douglas, A. G. A Pyrolysis-Gas Chromatographic Method for Kerogen Typing. In *Advances in Organic Geochemistry 1979*; Douglas, A. G., Maxwell, J. R., Eds.; Pergamon Press: Oxford, 1980; pp 579−584.
(63) Xiang, B.; Li, E.; Gao, X.; Wang, M.; Wang, Y.; Xu, H.; Huang, P.; Yu, S.; Liu, J.; Zou, Y.; Pan, C. *Org. Geochem.* **2016**, *98*, 1−17.
(64) Behar, F.; Kressmann, S.; Rudkiewicz, J. L.; Vandenbroucke, M. *Org. Geochem.* **1992**, *19*, 173−189.
(65) Prinzhofer, A. A.; Huc, A. Y. *Chem. Geol.* **1995**, *126*, 281−290.
(66) Espitalié, J.; Ungerer, P.; Irwin, I.; Marquis, F. *Org. Geochem.* **1988**, *13*, 893−899.
(67) Horsfield, B.; Schenk, H. J.; Mills, N.; Welte, D. H. *Org. Geochem.* **1992**, *19*, 191−204.
(68) Behar, F.; Hatcher, P. G. *Energy Fuels* **1995**, *9*, 984−994.
(69) Tang, Y.; Jenden, P. D.; Nigrini, A.; Teerman, S. C. *Energy Fuels* **1996**, *10*, 659−671.
(70) Behar, F.; Lewan, M. D.; Lorant, F.; Vandenbroucke, M. *Org. Geochem.* **2003**, *34*, 575−600.
(71) Lorant, F.; Behar, F.; Vandenbroucke, M.; McKinney, D. E.; Tang, Y. *Energy Fuels* **2000**, *14*, 1143−1155.
(72) Leininger, J-P.; Lorant, F.; Minot, C.; Behar, F. *Energy Fuels* **2006**, *20*, 2518−2530.
(73) Fusetti, L.; Behar, F.; Bounaceur, R.; Marquaire, P-M.; Grice, K.; Derenne, S. *Org. Geochem.* **2010**, *41*, 146−167.
(74) Alexander, R.; Berwick, L. J.; Pierce, K. *Org. Geochem.* **2011**, *42*, 540−547.
(75) Tegelaar, E. W.; Noble, R. A. *Org. Geochem.* **1994**, *22*, 543−574.
(76) Reynolds, J. G.; Burnham, A. K. *Org. Geochem.* **1995**, *23*, 11−19.
(77) Peters, K. E.; Burnham, A. K.; Walters, C. C. *AAPG Bull.* **2015**, *99*, 591−616.
(78) Ungerer, P.; Pelet, R. *Nature* **1987**, *327*, 52−54.
(79) Schenk, H. J.; Horsfield, B. *Geochim. Cosmochim. Acta* **1993**, *57*, 623−630.
(80) Peters, K. E.; Walters, C. C.; Mankiewicz, P. J. *AAPG Bull.* **2006**, *90*, 387−403.
(81) Vandenbroucke, M.; Largeau, C. *Org. Geochem.* **2007**, *38*, 719−833.
(82) Pepper, A. S. *Estimating of Petroleum Expulsion Behavior of Source Rocks: A Novel Quantitative Approach*; England, A. J., Fleet, A. J., Eds.; Petroleum Migration; Geological Society Special Publication, 1992; Vol *59*, pp 9−31.
(83) Pepper, A. S.; Corvi, P. J. *Mar. Pet. Geol.* **1995**, *12*, 417−452.
(84) Sandvik, E. I.; Young, W. A.; Curry, D. J. *Org. Geochem.* **1992**, *19*, 77−87.
(85) Song, W.; Jiang, T. *Natural Gas Industry* **2008**, *28* (10), 1−4 in Chinese.
(86) Zhao, M.; Lu, S.; Wang, T.; Li, J. *Chin. Sci. Bull.* **2002**, *47*, 113−119.

DOI: 10.1021/acs.energyfuels.6b01143
Energy Fuels 2017, 31, 73−94

(87) Liang, D.; Zhang, S.; Chen, J.; Wang, F.; Wang, P. *Org. Geochem.* **2003**, *34*, 873−888.
(88) Patience, R. L. Where did all the coal gas go? *Org. Geochem.* **2003**, *34*, 375−387.

DOI: 10.1021/acs.energyfuels.6b01143
Energy Fuels 2017, 31, 73−94